Carbohydrate Polymer Technologies and Applications 11 (2025) 100929

Contents lists available at ScienceDirect

Carbohydrate Polymer Technologies and Applications

journal homepage: www.sciencedirect.com/journal/carbohydrate-polymer-technologies-and-applications

Development of nanocellulose-hyaluronic acid bioinks for 3D bioprinting facial cartilages

Thomas H Jovic [a,b,*], Andrea Gazze [c], Bethan Morgan [c], Karl Hawkins [c], Lewis Francis [c], Hari Arora [d], Shareen H Doak [c], Iain S Whitaker [a,b]

[a] Reconstructive Surgery & Regenerative Medicine Research Centre, Swansea University, Swansea, UK
[b] Welsh Centre for Burns & Plastic Surgery, Morriston Hospital, Swansea, UK
[c] Swansea University Medical School, Institute of Life Sciences 2, Swansea, UK
[d] College of Engineering, Swansea University, Swansea, UK

ARTICLE INFO

Key words:
Cartilage
Bioprinting
Chondrogenesis
Nanocellulose
Hyaluronic acid
Biomaterials

ABSTRACT

Nanocellulose (NC) possesses desirable biological and mechanical properties for 3D bioprinting. This study aimed to derive a novel NC-hyaluronic acid (HA) bioink for 3D bioprinting facial cartilages and assess its printability, biocompatibility and chondrogenicity. Pulp-derived NC blend was combined with a HA hydrogel to make composite NCHA bioinks ranging from 100 % HA to 20 % HA. Human nasoseptal chondrocytes were cultured in the bioinks for 21 days to assess chondrogenicity through gene expression analysis, quantitative protein assays and histology. Successful crosslinking using hydrogen peroxide solution (5 μM) occurred within 5 min with no detriment to cell survival. All NCHA mixtures demonstrated increases in aggrecan, collagen and SOX9 expression over 21 days with bioinks comprising 20–40 % HA being the most chondrogenic ($p = 0.0001$). Printability was assessed using rheology and printability assays, demonstrating appropriate mechanical properties for 3D printing and shape retention as auricular cartilages. Biocompatibility with Live-Dead, lactate dehydrogenase and AlamarBlue assays demonstrated cell viability and proliferation sustained over 21 days. We conclude that NCHA bioinks promote chondrogenicity, possess favourable mechanical properties and have excellent biocompatibility for cartilage tissue engineering.

Introduction

Defects in facial cartilage can be associated with a significant psychosocial burden for patients, with many requiring reconstructive surgery to restore form and function (Jovic et al., 2018). Cartilaginous structures such as the ear and nose are especially challenging to reconstruct owing to their complex 3D geometry and unique structural and mechanical properties (Al-Himdani et al., 2017; Jessop et al., 2015). Autologous reconstruction, despite offering excellent results in many cases, demands extensive donor tissue to be harvested from the rib cage, and multiple lengthy operations for patients (Truong & Maricevich, 2017). As such there have been attempts to tissue engineer facial cartilages for use in reconstructive surgery for over 25 years (Jovic et al., 2020a; Malkoc, 2018). In particular, 3D bioprinting has gained significant traction owing to the ability to have greater macroscopic control over shape geometry and microscopically over tissue architecture and cellular placement, offering true personalisation for the intended recipient (Jovic et al., 2020b). However, efforts to date have been hindered by limitations in cell source and material selection leading to resorption, ossification, degradation and immunogenicity (Jessop, Al-Sabah et al., 2016, 2016; Jovic et al., 2020b).

Natural biomaterials have gained increasing interest owing to their unique combination of biomechanical strength and excellent biocompatibility, addressing many of the limitations of synthetic materials and possessing the potential to bypass the shortcomings of previous cartilage tissue engineering efforts (Jovic et al., 2019a; Tarassoli et al., 2021). Whilst natural materials may be more biomimetic, cartilage extracellular matrix is a heterogeneous substance, comprising a mixture of collagens, proteoglycans and glycoproteins (Jessop, Zhang et al., 2019; Vincent et al., 2022), meaning that true biological mimicry is likely to require a composite bioink containing more than one biomaterial (Heid & Boccaccini, 2020). Further advantages of the composite bioink approach include the ability to combine materials to enhance printing, shape fidelity, bioactivity and compatibility specific to the intended

* Corresponding author. Reconstructive Surgery & Regenerative Medicine Research Centre, Institute of Life Sciences 1, Swansea University, Swansea, UK, SA2 8PP.
E-mail address: t.h.jovic@swansea.ac.uk (T.H. Jovic).

https://doi.org/10.1016/j.carpta.2025.100929

Available online 30 June 2025

target tissue type.

We have previously demonstrated that pulp-derived nanocellulose (NC) is a natural biomaterial that can be produced in three distinct structural formulations: NC Crystals (CNC), Nanofibrillated Cellulose (NFC) and a unique NC Blend (NCB) comprising a naturally-occurring combination of crystalline and fibrillar components (Al-Sabah et al., 2019a; Jessop, Al-Sabah et al., 2019a; Jovic et al., 2023a; Kyle et al., 2018a). When blended with alginate, these biomaterials show promising properties for 3D bioprinting: excellent print resolution and fidelity and enhanced chondrogenic potential (Jessop, Al-Sabah et al., 2019a; Jovic et al., 2023a), mirroring previous studies of NC-alginate as a bioink (Apelgren et al., 2017; Markstedt et al., 2015; Möller et al., 2017; Müller et al., 2017).

Hyaluronic acid (HA) is a naturally occurring, anionic and non-sulphated glycosaminoglycan, and a major constituent of extracellular matrix, particularly in cartilage and skin. HA has a particularly prominent role in cartilage, owing to its biomechanical and physicochemical properties (Gupta et al., 2019), and confers key roles in cell proliferation, migration, differentiation and tissue morphogenesis (Fallacara et al., 2018), via cell-matrix interactions (Kiani et al., 2002). Many of these properties render HA an excellent biomaterial for use in biomedical applications, and indeed HA has been successfully translated into clinical uses such as in wound dressings, cosmetics and joint injections (Cooper et al., 2017; Fagien et al., 2019; Graça et al., 2020).

In addition to these structural properties and biocompatibility, there are further features of HA that render it a promising material for 3D printing applications. Specifically, the use of HA as a dermal filler has yielded interest from industry owing to its rheological properties and ease of injection (Fagien et al., 2019). This translates well to extrusion bioprinting, where shear thinning properties and viscoelasticity are mutually beneficial to both disciplines. The abundance of hydroxyl and carboxyl side chains also renders HA amenable to chemical, physical and enzymatic crosslinking, with value for improving shape fidelity post-3D bioprinting (Khunmanee et al., 2017a; Wu et al., 2016; Yu et al., 2013). However, a dominance of viscosity over elasticity, owing to its high water content, translates to poor shape retention post-printing (Petta et al., 2020a). This been addressed by structural modification of the HA hydrogels or through blending HA with natural or synthetic polymers to augment its printability (Poldervaart et al., 2017; Petta et al., 2018), with previous candidates including methacrylated gelatin and polycaprolactone (Hauptstein et al., 2020a; Khunmanee et al., 2017b; Petta et al., 2020b; Petta, Grijpma et al., 2018a).

We hypothesise that blending NC with HA would augment the printability and shape fidelity of HA bioinks, producing a composite capable of serving both the biological and mechanical roles of a bioink designed to print facial cartilages. Through an analysis of mechanical properties: rheology, printability and strength; and biological properties: chondrogenicity and biocompatibility; a thorough evaluation of the advantages and caveats of this biomaterial combination are presented.

Methods

Preparation of bioinks

A hydrophilic NC blend (NCB, containing components of both Cellulose Nanocrystals and Nanofibrillated Cellulose) was used in the development of the composite bioink, derived from softwood biomass using American Value Added Pulping (AVAP) biorefinery technology (Nelson & Restina, 2014). The NCB formulation has been extensively characterised in our previous work (Al-Sabah et al., 2019b; Jessop, Al-Sabah et al., 2019b; Jovic et al., 2023b; Kyle et al., 2018b) and comprises 5 % w/v NC powder, comprising pure cellulose I of a mean fibril length of 925±787 nm and width of 17±12 nm (Kyle et al., 2018b). in distilled water (BioPlus, GranBio, GA, USA). This was sterilised with steam autoclave at 126 °C for 20 min using a desktop autoclave (Prestige Medical, Blackburn, UK) as previously described (Al-Sabah et al., 2019a).

Non-sulphated hyaluronic acid powder of mixed molecular weights with a 5 % tyramine substitution (HA) was purchased from LifeCore Biomedical (Corgel 5 %; Chaska, MN, USA). The HA powder was dissolved in sterile horseradish peroxidase in PBS (10 U/mL; LifeCore, MN, USA) to produce a hydrogel with concentration of 30 mg/ml.

Composite NC-hyaluronic acid (NCHA) bioinks were produced using NCB and the 5 % Tyramine-substituted HA hydrogel. NCHA bioinks were produced in a series of formulations as outlined in Table 1.

Rheological characterisation of NCHA composite bioinks

Rheological analysis of the materials in their uncrosslinked, hydrogel states was performed using an AR-G2 Controlled Stress Rheometer (TA instruments, New Castle, DE, USA) with the bottom plate set at a temperature of 22 °C. Samples of each hydrogel of interest (100HA – 20HA) were analysed using an initial frequency sweep with a range of 0.1 to 10 Hz maintained at 0.5 Pa stress. All measurements were within the linear viscoelastic range of the samples. The values of storage modulus (G'), loss modulus (G") and complex modulus (G*) were also recorded throughout this frequency range. The loss tangent (tanδ) was calculated from G"/G'. The sample was allowed to equilibrate for 10 s prior to commencing a shear flow ramp analysis, in which logarithmically increasing shear rates of 0.1–100 s^{-1} were exerted over a two-minute period. Each hydrogel was tested by using separate samples in triplicate.

Crosslinking optimisation

NCHA bioinks were crosslinked using hydrogen peroxide solution (LifeCore Biomedical, MN, USA). The hydrogen peroxide was diluted in PBS (Sigma Aldrich, MO, USA) to provide a range of biocompatible concentrations consistent with the doses reported in the literature (Khan et al., 2008; Martin et al., 2005). Specifically, solutions of 5, 10, 15 and 20 μM were used and compared to the optimal dose recommended by the manufacturers of 0.391 % (115 mM) as a positive control. The optimum duration of crosslinking was determined using a rheometer, in which the storage and loss moduli were measured continuously post-application of the crosslinking agent for a total of 840 s (14 min).

Printability assessment

A CELLINK INKREDIBLE extrusion bioprinter (CELLINK, Gothenburg, Sweden) was used to assess the printability of the bioink. The minimum extrusion pressure of each material was determined by gradually increasing the extrusion pressure from 0 kPa until the minimum pressure at which the bioink was deposited continuously through a 22 G nozzle. An STL file of a human auricle was used to print a 3D ear in the NCHA bioink and compared to a control auricle of the same design printed in PLA using an Ultimaker 3 Printer (Ultimaker, Utrecht, NL).

iCELLigence cytotoxicity assay

The iCELLigence apparatus (Agilent Technologies, CA, USA) was used to assess for changes in cell adherence and growth following exposure to different doses of hydrogen peroxide crosslinking agent.

Table 1
NCHA composite bioinks with percentage v/v of each constituent and their associated nomenclature.

Bioink Name	Volume NCB (%)	Volume Tyramine-substituted HA (%)
100HA	0	100
80HA	20	80
60HA	40	60
40HA	60	40
20HA	80	20

17,500 human nasoseptal chondrocytes were seeded into the wells of an iCELLigence E8 plate and allowed to adhere and proliferate in standard culture conditions. Two wells were used as media only controls. Adherence and baseline proliferation were measured over 18 h, measured once per minute for the first two hours and then hourly for the remaining 16 h. At the 18 hour time window, the impedance readings were paused, the media was removed from the cells, and 200 µl of warm PBS or warm hydrogen peroxide was added to each well and left at room temperature for five minutes. The hydrogen peroxide was thereafter discarded and the wells were washed three times with warm PBS, after which fresh 500 µl medium was added to the wells. Measurements were then taken every minute for two hours to accurately capture the immediate cytotoxic window, and then hourly until a total experimental time of 70 h was attained.

The change in cellular impedance after exposure to the peroxide was used to calculate a percentage of cell death corrected to the change observed in the PBS control. Growth curves after the addition of peroxide were also monitored and compared between doses. Technical duplicates were performed on biological triplicates.

AlamarBlue assay

Cellular metabolism of the alamarBlue dye (ThermoFisher Scientific, MA, USA) was used to provide an indication of cell proliferation. A 10 % (v/v) alamarBlue solution was made by adding the solution to media, co-cultured with cells ± material for 4 h. The colorimetric change was quantified using a plate reader to detect absorbency at 570 nm (reduced form) and 600 nm (oxidised form) wavelengths, along with media only controls (no cells), taken after 4 h. The two wavelength readings for each well were used to calculate the percentage of the reacted alamarBlue solution as a marker of cell metabolic activity and number.

Lactate dehydrogenase (LDH) assay

Three media samples were taken immediately after exposure to the hydrogen peroxide reagents from three biological triplicates, after which point, media was reapplied to the wells and left for four hours. One well treated with PBS only was spiked with cell lysis buffer (Thermofisher Scientific, MA, USA) and used as a positive control for cytotoxicity, assumed to have 100 % lysis. 50 µl samples from each well were mixed with reaction media for 30 min. The reaction was stopped after 30 min using stop solution and the plates were read immediately at 490 nm and 680 nm as per manufacturer guidance (Thermofisher Scientific, MA, USA). Percentage of cytotoxicity was calculated relative to the spiked control.

Live-Dead assay

The live-dead mammalian cell viability assay kit (Thermofisher Scientific, MA, USA) was used to visualise live and dead cells within biomaterials and in cell culture conditions following exposure to hydrogen peroxide. A solution of PBS containing 1:1000 Calcein-AM dye and 1:500 Ethidium homodimer-1 was added to the cells or cell-laden biomaterials, protected from light and left to incubate in standard culture conditions for 45 min. The cells and pellets of interest were visualised under fluorescent microscopy using an inverted microscope (Olympus Ixplore, Olympus, Tokyo, Japan). 3 to 4 representative points were captured per sample, and at different depths at 10x magnification.

Atomic force microscopy

100 µl of acellular crosslinked biomaterial were immersed in media for 24 h under standard culture conditions. After 24 h, the biomaterial discs were then secured onto the base of a microscope cover slip with a single drop of mounting medium (VWR, PA, USA). The surface topography and elastic modulus of each biomaterial was investigated using a Bruker BioScope Catalyst Atomic Force Microscope (Bruker, MA, USA) with MikroMasch cantilevers CSC37 (Mikromasch, Tallinn, Estonia). Parameters used were a nominal radius of 8 nm, a nominal resonance frequency of 20 kHz and a nominal spring constant of 0.3 N/m. The cantilevers were pre-calibrated on a glass slide to determine the experimental deflection sensitivity and spring constant.

Force curves were acquired on each biomaterial using a maximum force of 4 nN to allow the elastic modulus of the biomaterials to be calculated. The elastic modulus was calculated using the Sneddon model in the Nanoscope Analysis software (v1.50, Bruker, MA, USA).

A minimum of 50 data points were collected for each biomaterial sample. Topographical analysis was acquired in PeakForce Quantitative NanoMechanics (QNM) mode (Bruker, MA, USA).

Porosity and swelling assays

100 µl discs of biomaterial were produced in triplicate and crosslinked using 100 µl of crosslinking agent. The discs were weighed (m_{wet}) and added to a 48 well plate with 1 ml PBS. The 48 well plate was incubated at 37 °C and 5 % CO_2 for 24 h. Thereafter, the fully hydrated weight of the discs was obtained ($m_{fully\ hydrated}$). The swelling was calculated using the following formula:

$$\text{Swelling } \% = \frac{m_{fully\ hydrated} - m_{wet}}{m_{wet}} \ x\ 100$$

To calculate porosity, 100 µl discs of biomaterial were crosslinked in triplicate. The discs were left at room temperature for 24 h in 1 ml PBS. Each disc was weighed after blotting and recorded as m_{wet}. The discs were transferred to a dry 37 °C chamber for 72 h. The discs were weighed thereafter and recorded as m_{dry}. Porosity (%) was calculated using the following formula:

$$\text{Porosity } = \frac{m_{wet} - m_{dry}}{\rho_{PBS}\ x\ V_{pellet\ fully\ swollen}} \text{x100}$$

Where ρ = is the density of PBS at 20 °C (1.0723 g/cm^3).

Cell culture and isolation

Human nasoseptal chondrocytes (hNSCs) were acquired from waste tissue following septorhinoplasty procedures after informed patient consent (IRAS ID 99,202). A total of three biological repeats (three patient samples) were acquired. Cartilage tissue was digested in 0.4 % pronase (Roche, UK) for 1 hour followed by 0.2 % collagenase type I solution for 16 h (Sigma-Aldrich, Poole, UK) at 37 °C, 5 % CO_2 and with gentle agitation. The resultant cell suspension was strained, centrifuged and cultured in 5 % CO_2 at 37 °C. Culture medium used for all conditions consisted of Dulbecco's Modified Eagle Medium, no glucose (Sigma-Aldrich, Poole, UK) supplemented with 10 % fetal bovine serum (Sigma-Aldrich, Poole, UK), 100 µg/ml penicillin and 100 U ml−1 streptomycin (Sigma-Aldrich, Poole, UK), 1 mM glucose (SigmaAldrich, Poole, UK), and 0.1 % non-essential amino acids (Thermo Fisher Scientific, Paisley, UK), and was changed every 2–3 days. Cells were allowed to expand up to 70 % confluence prior to passage with 0.05 % trypsin-EDTA (Thermo Fisher Scientific, Paisley, UK). Cell counts were performed using trypan blue exclusion (Thermofisher Scientific, MA, USA). Passage 2 cells were used at a seeding density of 3 × 10^6 cells per ml within 100 µl of crosslinked biomaterial to protect chondrogenic phenotypes, as dedifferentiation was observed at higher passages (Jovic et al., 2024). Constructs were immersed in the aforementioned media for 21 days, with media changes every 3 days.

Chondrogenic gene expression analysis

RNA was extracted from biomaterials as previously described (Jovic et al., 2023b). The RNA was converted to cDNA using reverse transcription, and quantified for the expression of COL2A1, SOX9 and

ACAN1 relative to housekeeping gene expression (TBP). Each material was harvested for RNA extraction and PCR analysis at 4 h (Day 0), 7 days, 14 days and 21 days of culture using 3 biological repeats. All relative gene expression values were expressed as fold-changes using the ΔΔCt method (Livak & Schmittgen, 2001) compared to a control value: in this case 100HA at the 4-hour time point.

Extracellular matrix analysis

10 mg of each cell-laden material was analysed for hydroxyproline content as a marker of collagen production. Samples were homogenised and hydrolysed using 12 M hydrochloric acid at 120 °C for 3 h and centrifuged at 10,000 g for 3 min. 10 μl of the supernatant was analysed in triplicate along with one spiked sample and a set of hydroxyproline standards and evaporated at 60 °C. 100 μl of Chloramine T and oxidation buffer (Sigma Aldrich, US) was added to each well and left for 5 min, with a further 100 μl mixture of DMAB reagent diluted in perchloric acid and isopropanol added thereafter for 90 min at 60 °C. The plates were then read at 560 nm absorbance using a plate reader (POLARstar Omega spectrophotometer, BMG LABTECH, Ortenberg, Germany).

The dimethylmethylene blue (DMMB) assay was used to quantify glycosaminoglycan content in each material at 7 days and 21 days of culture. The cell-laden bioinks were first digested using 300 μl of a 10 mg/ml solution of type I hyaluronidase (Sigma Aldrich, US) at 37 °C for 1 hour. Isolates were diluted 1 in 50 with distilled water and added to the wells of a 96 well plate in triplicate with 200 μl DMMB reagent. The plates were read immediately at 525 nm compared to a series of chondroitin standards ranging from 0 to 50 μg/ml.

Histological analysis was performed to visualise extracellular matrix deposition relative to chondrocytes. Cell-laden biomaterial hemispheres were immersed in 4 % paraformaldehyde solution for 30 min and then washed three times in PBS. The constructs were then immersed in either 1 % (w/v) Alcian Blue stain for 30 min; 0.1 % toluidine blue solution for 10 min or Safranin O using first Fast green for 20 min, washed with acetic acid and stained thereafter with Safranin O stain for 40 min. The constructs were viewed under brightfield microscopy at 4, 10 and 20x magnification with images taken throughout the construct (in x, y and z axes) to ensure the images captured were representative of the whole material.

Biomechanical compression testing

200 μl cylindrical disks of each biomaterial were produced of 6 mm diameter and 7 mm length. The materials were crosslinked using 5 μM H_2O_2 for five minutes and transferred in PBS for compression testing. The 1ST Mechanical Compression Device (Tinius Olsen, Redhill, UK) mounted with a 25 N load cell was used to perform compression testing. Each material was blotted dry with tissue paper and compressed to determine the break distance, break force and ultimate compressive strength. These values were used to calculate the ultimate mechanical stress, break stress and strain to failure of each material. Materials were examined without cells (in technical triplicates), and then after culture with cells for 21 days (in technical triplicates) to determine whether the cells and the matrix they produced had any significant effect on the mechanical properties of the material.

Statistical analysis

A total of three biological repeats were used in this study, with technical repeats conducted in at least triplicate (duplicate for iCELLigence experiments as described). Datasets were assessed for normality (Gaussian distribution) visually and, where possible, using an Anderson-Darling test. All data presented is the mean value of technical ± biological replicates which is presented graphically with error bars depicting standard deviation unless otherwise stated.

The following data sets were analysed using unpaired, two tailed *t*-tests: PCR data, where expressed relative to an initial, control time point. A one-way ANOVA was used with a Tukey's post hoc test for multiple comparisons for: Line fidelity assays; porosity, swelling and crosslinking changes; 21-day gene expression data for cartilage markers. A Kruskal Wallis ANOVA with Dunn's post hoc test was used for Young's modulus from AFM data owing to non-Gaussian distribution.

A 2-way ANOVA with a Tukey's post hoc test was used for biomechanical compression tests, AFM data with/without cells and AlamarBlue Assays.

Results

In order to validate the suitability of NCHA bioinks for 3D bioprinting facial cartilage tissue, we outline our optimisation of NCHA composites from 20HA (20 %HA to 80 % NC) to 100HA (100 % HA, 0 % NC) through an assessment of printability, crosslinking potential and chondrogenic potential to determine the most appropriate formulation for progressing towards clinically translatable bioengineered facial cartilages.

Rheological characterisation of NCHA bioinks

Rheological analysis provides insight into the suitability of bioinks for extrusion-based bioprinting.

Each bioink was then assessed for their storage (G'), loss (G") and complex modulus (G*) in their non-crosslinked hydrogel formulations (1A-C). Of note, the bioinks with a dominance of NC in their composition (20HA, 40HA) had higher G' than G" moduli, and as a result a higher G* modulus. Furthermore, the loss tangent of the 20HA and 40HA bioinks was consistently <1, indicating a dominance of viscoelastic solid behaviour. There were no statistically significant differences noted in the storage modulus ($p = 0.4$), complex modulus ($p = 0.4$) or loss tangent ($p = 0.6$) between the 20HA and 40HA materials, but the loss modulus of 40HA was significantly higher than 20HA ($p = 0.0003$).

Conversely, the G' and G" were more closely aligned in 60HA with an overall minor dominance of G' and a loss tangent of <1 at the frequencies tested, meaning a dominance of elastic over viscous type behaviour was also observed in this bioink. The loss tangent was significantly higher than 20HA ($p = 0.0006$) but not 40HA ($p = 0.3$) meaning a significantly greater degree of viscosity and lesser elasticity was observed compared to 20HA but not 40HA The complex, storage and loss moduli were significantly different between both 20HA and 40HA with 60HA however.

The inverse of these phenomena was observed in 80HA and 100HA, where a higher G" than G' was observed, and a loss tangent greater than 1 was seen at the majority of the frequencies tested, indicating a prevalence of viscous, liquid-type behaviour. These bioinks are as such, liable to deformation owing to a lack of elasticity relative to viscosity, with implications for bioprinting. The loss tangent of 80HA and 100HA were significantly higher than both 20HA and 40HA ($p < 0.0001$). Despite all bioinks possessing printability potential, the complex modulus of the 20HA and 40HA formulations therefore appear most favourable for extrusion bioprinting. Shear rate ramps were performed to determine the flow properties of the different NCHA formulations by measuring the viscosity of the inks as a function of increasing shear rate. All of the material blends demonstrated shear thinning behaviour making them suitable candidates for extrusion based bioprinting (Fig. 1D).

In order to characterise the maximum amount of time for crosslinking changes to occur, the weakest crosslinking combination: 20HA with 5 μM of H_2O_2, was used to quantify the change in the material's mechanical properties with time after application of crosslinking agent. Throughout the time period studied, the loss modulus remained below 1 indicating a dominance of elastic over viscous behaviour, with the greatest changes in stiffness observed within the 5-minute window (300 s; Fig. 2). As such, five minutes of exposure to the crosslinking agent was

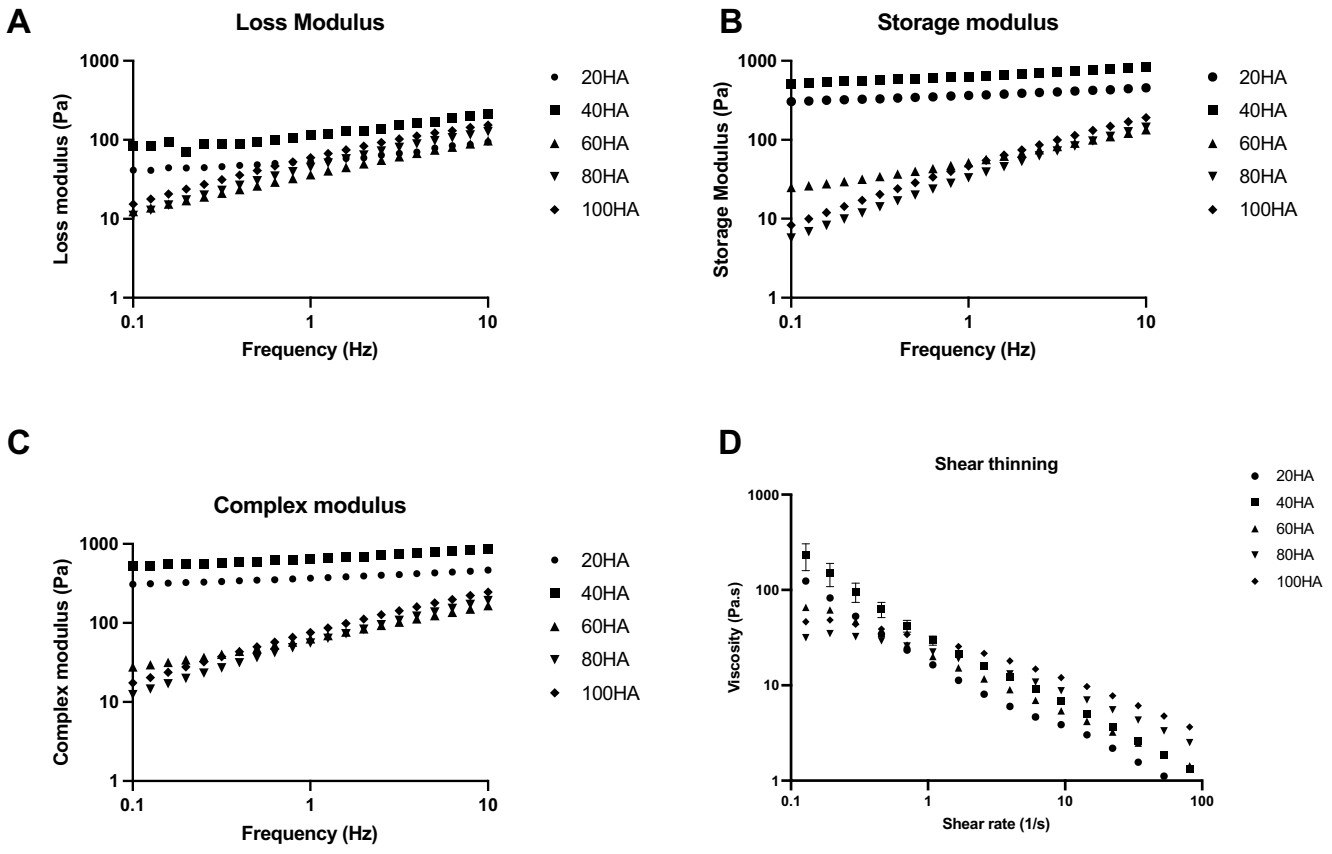

Fig. 1. Rheological analysis of NCHA composite bioinks and 100HA, each point represents a mean value of 3 separate readings. A) Loss modulus (G") is plotted on logarithmic axes as a product of frequency in which a dichotomy between 20–40HA and 60–100HA is highlighted. B) Storage modulus (G') is plotted logarithmically against frequency showing minimal change in G' across the frequency range studies in 20HA and 40HA C) Complex modulus (G*) for each NCHA bioink formulation is plotted logarithmically as a function of increasing frequency mirroring the findings of A) and B) in which 20HA and 40HA show minimal change in G* across the frequency range used. D) Shear thinning of NCHA composite bioinks. Viscosity in Pa.s is plotted against shear rate for each NCHA bioinks in which 20 = 20HA, 40=40HA, 60=60HA, 80=80HA and 100=100HA Shear thinning (a reduction in viscosity with increasing shear) can be observed in all bioinks.

used hereafter.

Biocompatibility of crosslinking

The Tyramine substitution on the HA chains renders the HA within the NCHA hydrogels capable of covalent crosslinking in the presence of hydrogen peroxide and horseradish peroxidase enzymes. However, the free radical generation during this process may be cytotoxic and genotoxic at high doses. A range of potentially biocompatible doses between 5 and 20 μM were used in line with ranges deemed suitable for chondrocytes reported in the literature (Khan et al., 2008; Martin et al., 2005) over a five-minute crosslinking window.

Chondrocytes displayed good viability at doses of 5–20 μM hydrogen peroxide (Fig. 3A–D) but complete cell death was observed at 115 mM (0.39 %) hydrogen peroxide doses (Fig. 3E) using the live:dead assay.

In addition to the immediate cytotoxic potential of peroxide, the impacts on cellular proliferation and metabolism were explored using iCELLigence (Fig. 3F–G). Over a period of 24 h, similar growth curves were observed in all wells prior to the addition of hydrogen peroxide. Thereafter, all groups experienced a change in cell impedance with no statistically significant differences observed between the 0, 5 ($p = 0.06$) and 10 μM ($p = 0.3$) groups. The effect of 115 mM was so deleterious to cells that no significant differences were observed between this dose and media only ($p > 0.999$). 20 μM was also significantly worse than not only the PBS control (0 μM, $p < 0.0001$), but also 5 μM ($p = 0.0004$) and 10 μM ($p < 0.0001$) during the cytotoxic event window. Cellular metabolic activity after exposure to peroxide was examined using the alamarBlue assay (Fig. 2I). Significantly lower metabolic activity was observed over the course of 4 h in the 0.39 % (115 mM) group (52.9 %; $p < 0.0001$) relative to all other doses used. The 15 μM dose (86.7 %) was also significantly lower than 5 (93.5 %, $p = 0.03$) and 10 μM (93.7 %, $p = 0.02$) but there were no significant differences seen between the other doses of hydrogen peroxide used.

To assess for delayed cell death, the LDH assay was used immediately and at 4 h. Statistically significant differences in cytotoxicity were observed between the 115 mM doses and 0 μM (PBS control) immediately ($p < 0.0001$) and at 4 h after exposure ($p < 0.0001$) and at 20 μM (7.3 % immediately; 11.9 % at 4 h; $p = 0.03$). There were no significant differences observed with any other doses of peroxide used (Fig. 2H). Furthermore, there were no significant increases in cytotoxicity seen over the course of 4 h after exposure for any of the doses analysed.

In summary, doses of up to 10 μM of H_2O_2 were deemed to be biologically safe doses for use with human chondrocytes, with no adverse effects to cell proliferation or viability noted compared to control conditions.

Effect of crosslinking dose on structural properties

As 5–10 μM appeared the most biologically suitable doses for crosslinking, an assessment of the biomechanical suitability of this concentration is warranted, in particular when compared to the recommended crosslinking strength of 115 mM hydrogen peroxide for the

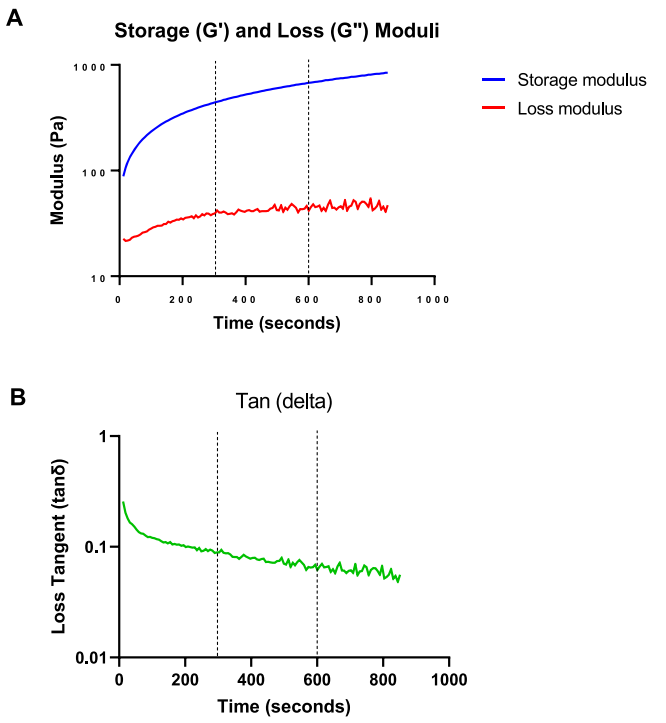

Fig. 2. Rheological characterisation of crosslinking time of 20HA with 5 μM H_2O_2. A) Loss modulus and storage modulus are plotted logarithmically against time (seconds) with dotted vertical lines indicating the 5 and 10 min marks. Evidence of a plateau is seen in the loss modulus as early as 5 min and a reduction in the gradient of the storage modulus is seen after both the 5 and 10 min marks. B) Loss tangent is plotted logarithmically against time in seconds with dotted vertical lines indicating 5 and 10 min marks. The curve shows a dominance of elastic over viscous behaviour (tanδ<1) with a minimal change noted after 5 and 10 min.

HA biomaterial.

Using uniaxial compression loading, there was a higher mean strain to failure value (Fig. 4A) in the low dose (5 μM) crosslinked material (64.7 %) compared to the high dose (115 mM) material (60.8 %), however this was not a statistically significant difference ($p > 0.999$). Similarly, a maximum compressive stress of 388.6 kPa was observed in the low dose group, compared to 421.3 kPa in the high dose group, but again this was not a statistically significant difference ($p = 0.5$) (Fig. 4B). The break force was slightly higher in the high dose crosslinked group at 2.26 N compared to 2.14 N but this was also not significant ($p = 0.8$).

Porosity and swelling assays were performed to determine how the effect of high dose and low dose crosslinking strengths affected the volume of the pores forms between the crosslinked bonds and how this affected the amount of liquid content the material accommodates in the form of swelling (Fig. 4D, 4E). A statistically significant difference in porosity was noted between the high dose and low dose crosslinking agent, with a mean porosity of 59.2 % in the low dose crosslinked material and 76.1 % in the high dose crosslinked material ($p = 0.03$). On a related note, from their completely dehydrated forms, the crosslinked hydrogel formulations displayed swelling in the region of 1500 to 2000 % indicating a high degree of water content. The degree of swelling was greater in the 20HA crosslinked with high dose peroxide (2028 %) compared to the low dose crosslinker (1711 %) but this was not significant ($p = 0.25$).

AFM was used to characterise the surface topography and stiffness of the NCHA in the presence of low (5 μM) and high (115 mM) dose crosslinking agents. A mean elastic (Young's) modulus of 11.8 kPa (median 8.45) in the low dose crosslinked material was observed compared to 23.5 kPa (median 7.65) in the high dose crosslinked material, though this was not a statistically significant difference ($p = 0.67$) (Fig. 4C). Topographically, a similar arrangement of surface fibres was observed in both crosslinking doses, displaying multidirectionality of fibres and interconnecting pores of variable sizes and depths. There was a degree of surface roughness in the low dose crosslinked material (Fig. 4F), where depths demonstrated a peak of 864 nm and trough of −771 nm (range of 1.6 μm) across a representative 15 μm area. Conversely, the higher dose crosslinked material (Fig. 4G) has much greater range of depths, observed across a 15 μm area with a peak height of 2.5 μm and trough of −2.3 μm (range 4.8 μm).

In summary, despite the detrimental cytotoxic effects of the high dose crosslinking agent, high dose crosslinking appears to significantly increase the porosity but not the swelling, compressive strength or the elastic modulus of the 20HA bioink. As there is minimal structural or mechanical benefit to using this dose, 5 μM H_2O_2 was used hereafter for crosslinking.

Effect of bioink composition of mechanical and structural properties of NCHA bioink

To test the suitability of the optimised crosslinking dose and timing on the different NCHA formulations, 100 μl hemispheres of the different NCHA composite biomaterials were produced and crosslinked in 5 μl H_2O_2 for 5 min. The change in the diameter of the hemispheres was calculated as a percentage change in diameter as seen in Fig. 5A. The highest change in diameter was observed in the 20HA material (−6.2 %), which was a significantly greater change than 100HA (−5.8 %; $p = 0.001$) and 80HA (−5.9 %; $p = 0.008$). Statistically significant differences were also observed between 40HA (−6.1 %) and 100HA ($p = 0.006$). Of note there were no statistically significant differences between the change in diameter post-crosslinking with 20HA, 40HA and 60HA (−6.0 %).

Porosity and swelling assays were undertaken to determine the water retention and pore sizes of the different NCHA formulations (Fig. 5B, 5C). The crosslinked hydrogels were highly hydrophilic, enabling swelling in the region of 2000 % in the 100HA (2016 %) and 20HA (1954 %) materials. Of note, there was lesser swelling noted in the 80HA (141 %), 60HA (172 %) and 40HA (548 %) materials, of which 80HA and 60HA were significantly lower than 20HA ($p = 0.0007$, $p = 0.0001$ respectively). The lower degree of swelling in these materials may be a reflection of the increased heterogeneity and surface charges of the material compositions.

Of all the materials tested, the 40HA appeared to have the highest ultimate stress value of 0.498 MPa (Fig. 5D), which was significantly stronger than 60HA (0.116 MPa, $p = 0.0001$) and 100HA (0.134 MPa, $p = 0.0002$). 20HA (0.389 MPa) was also stronger than these two materials (vs 60HA, $p = 0.0049$; vs 100HA $p = 0.009$) but not statistically different in strength to 40HA ($p = 0.5$). Of all the NCHA materials, 100HA was subjected to the least ultimate strain under compression, with a value of 39 % (Fig. 5E). This was statistically significant compared to 60HA (62.3 %; $p = 0.007$) but not to any other materials. The break force was determined in Newtons (Fig. 5F), and found to be greatest in the 40HA material (2.8 N), which was statistically significant compared to 60HA (0.74 N, $p = 0.0057$) and 100HA (0.87 N, $p = 0.0089$), but not to 20HA (2.14 N, $p = 0.56$) or 80HA (2.46 N, $p = 0.92$).

In summary, the most favourable mechanical properties were observed in the materials with at least 40 % (v/v) of NC. However, at higher proportions of NC (20HA), this was also associated with significantly higher water content (swelling) and a greater degree of contracture post-crosslinking.

Chondrogenic potential of NCHA bioinks

Chondrogenic gene expression

Firstly, gene expression was explored over a 21-day period for chondrogenic markers. Specifically, the genes used were SOX9, type II collagen (COL2A1) and aggrecan (ACAN1).

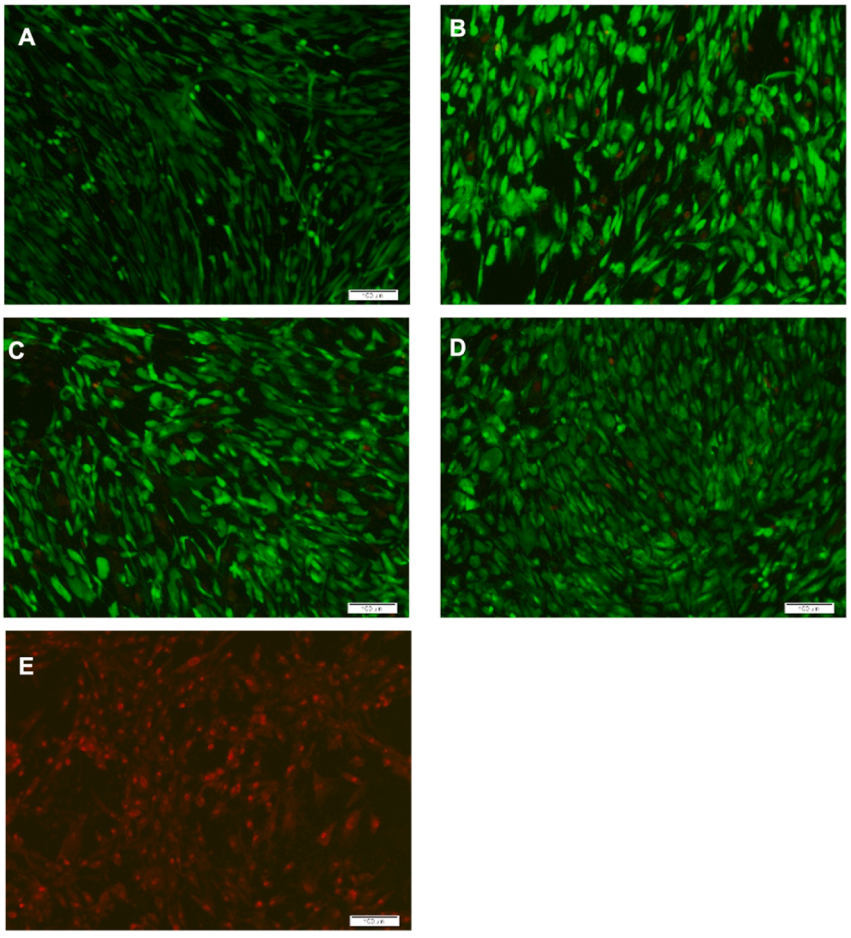

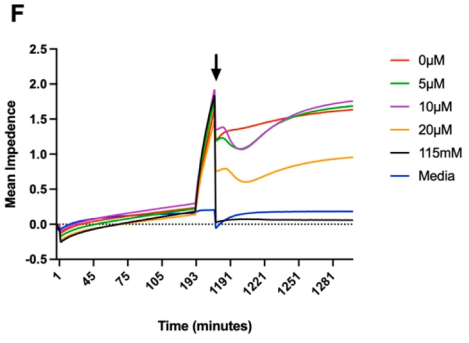

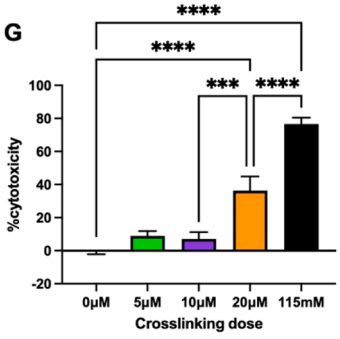

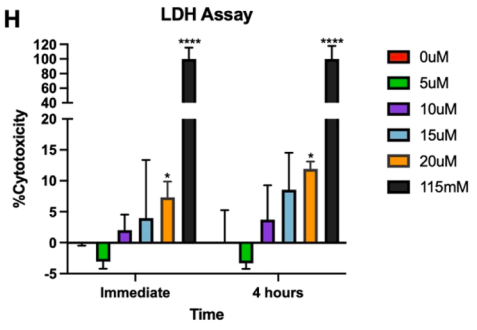

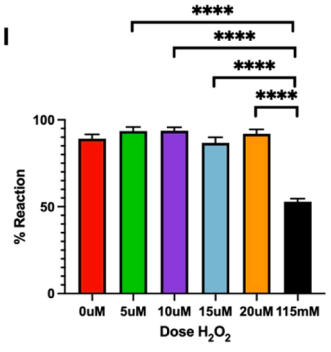

(caption on next page)

Fig. 3. A-F) Live-Dead Assay of chondrocytes exposed to different doses of H_2O_2. Live cells are coloured green, dead cells are coloured red. Representative images of 3 repeats taken at 10x magnification are displayed with scale bars depicting 100 μm. A) Live dead assay of chondrocytes exposed to PBS only (0 μM), universal cell survival is observed. Chondrocytes exposed to 5 μM (B), 10 μM (C) and 20 μM (D) H_2O_2, demonstrating predominant cell survival but a small number of dead cells. (E) Chondrocytes exposed to 115 mM H_2O_2 display universal cell death. F) Cell growth and subsequent changes in cell impedance following exposure to H_2O_2 for 5 min (point of addition demarcated with arrow). G) Percentage of cytotoxicity based on cell impedance before addition of peroxide and corrected for control (0 μM). H) Lactate Dehydrogenase (LDH) Assay of human chondrocytes immediately (left) and 4 h (right) after exposure to hydrogen peroxide expressed as a percentage of cell death (cytotoxicity). Mean values from 3 biological repeats in technical triplicate are presented. I) AlamarBlue Assay to show cell viability (expressed as a % of reacted alamarBlue reagent reacted) 4 h after of exposure to hydrogen peroxide. Mean values of 3 biological repeats + SD are presented. *=$p < 0.05$; **=$p < 0.01$; ***=$p < 0.001$; ****=$p < 0.0001$.

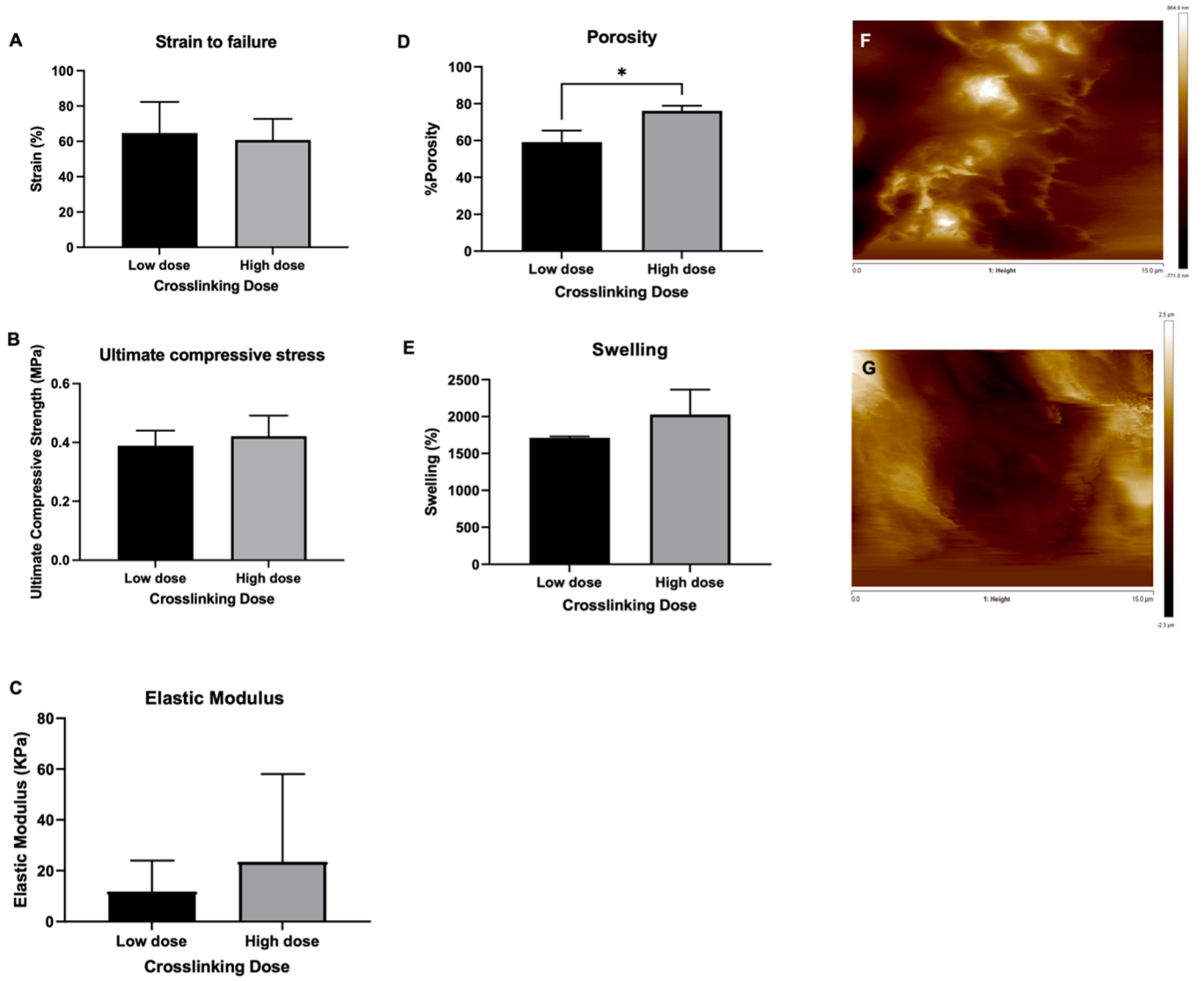

Fig. 4. Comparison of biomechanical properties of high (115 mM) and low dose (5 μM) crosslinked NCHA. Mean values of 6 repeats are presented with error bars depicting standard deviation. A) Strain to failure under compression is expressed as a mean percentage. No significant differences were observed between the two conditions. B) Mean maximum compressive stress is expressed in MPa. No significant differences were observed between the two conditions. C) Elastic modulus (kPa) of 20HA crosslinked with low dose (5 μM) or high dose (115 mM) peroxide crosslinking agent. Mean values of 162 measurements from 2 technical replicates are presented with error bars depicting the standard deviation. D) The percentage porosity of low dose and high dose crosslinked 20HA material are presented demonstrating a higher degree of porosity in the high dose crosslinked material. E) Swelling of NCHA material in high and low dose crosslinked groups from fully dehydrated state. No significant differences were observed between the two crosslinked states. F-G) Surface topography images of 20HA material acquired with AFM images. representative images are presented from 2 repeats of each condition. F) demonstrates a representative image of the low dose crosslinking agent. Depth is displayed on the scale on the right of each image and a scale bar is present beneath each image (15 μm). Shallow pores of varying sizes are demonstrated (1–10 μm) with a degree of surface roughness evident. G) depicts a representative image of the high dose crosslinking agent in which a greater degree of surface homology is observed but with larger, deeper pore sizes of approximately 10 μm width and 5 μm deep are demonstrated. Moderate surface roughness is also demonstrated.

COL2A1 gene expression showed significant increases over the course of 21 days in all bioinks (Fig. 6A). The greatest magnitude of change was observed in 80HA at 14 (370-fold, $p < 0.0001$) and 21 days (502-fold, $p < 0.0001$). The initial expression of COL2A1 was lower at the 4-hour timepoints in 40HA (0.55, $p = 0.04$) and 20HA (0.41, $p = 0.03$) materials and the 60HA at 24 h (0.29, $p = 0.008$). By Day 7, all

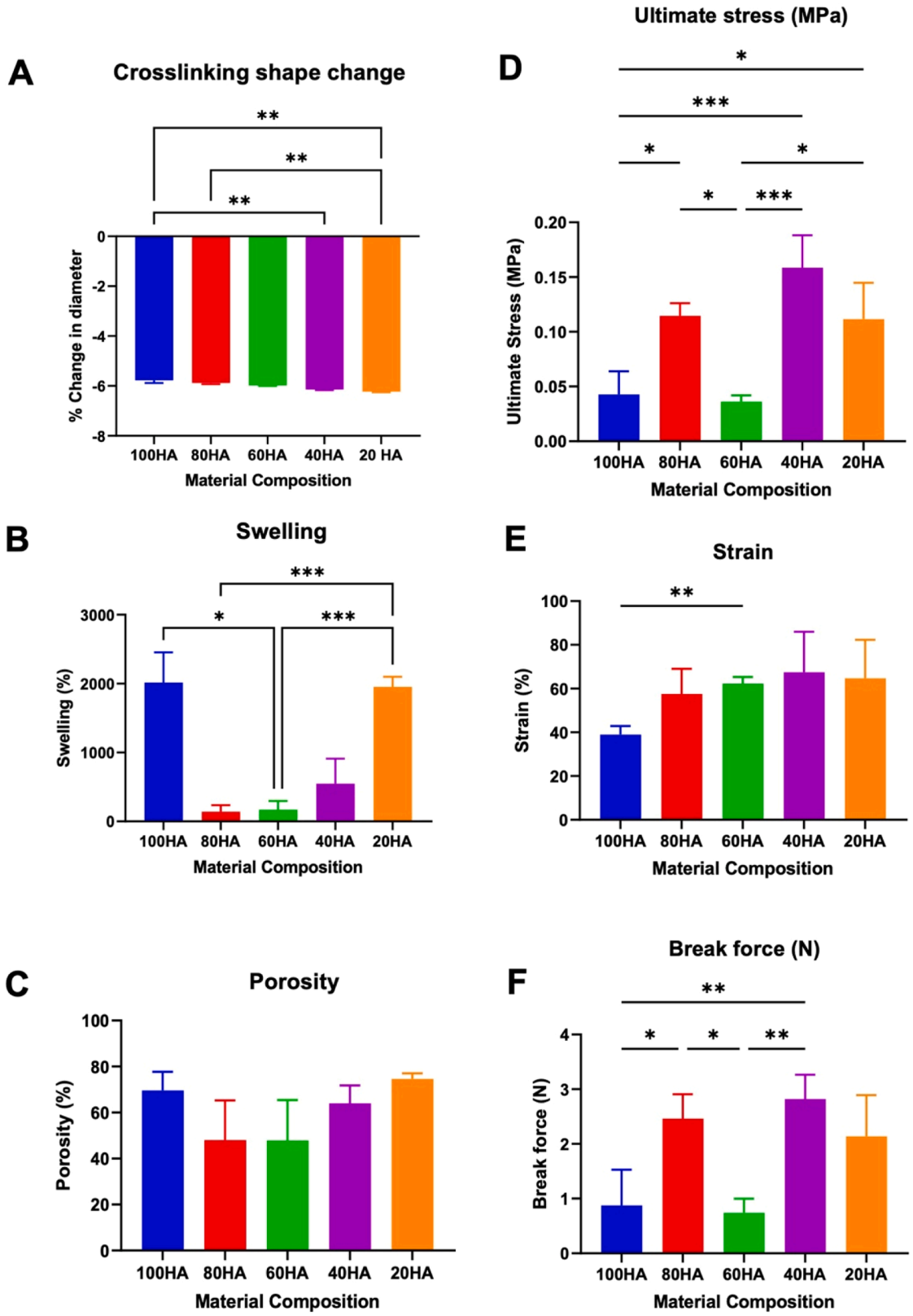

Fig. 5. A) Change in diameter of NCHA hemispheres following immersion in crosslinking agent. Mean values as a % change in diameter +SD are expressed for 3 repeats. B) Swelling of crosslinked NCHA bioinks. Values represent the mean of 6 repeats, expressed as a percentage from dry to fully hydrated mass + standard deviation. C) Porosity of crosslinked NCHA bioinks. Values represent a mean of 6 repeats + standard deviation expressed as a percentage of the total material. No significant differences were observed between material composition porosities. D) Ultimate compressive stress (MPa) is presented graphically demonstrating the highest compressive strength in 40HA, 20HA and 80HA relative to the 100HA and 60HA formulations. B) Strain to failure (expressed as a percentage) was comparable between all NCHA composite inks but significantly lower in the 100HA formulation relative to 60HA C) The break force of each material is presented in Newtons and demonstrates the highest break force in the 40HA and 80HA materials.

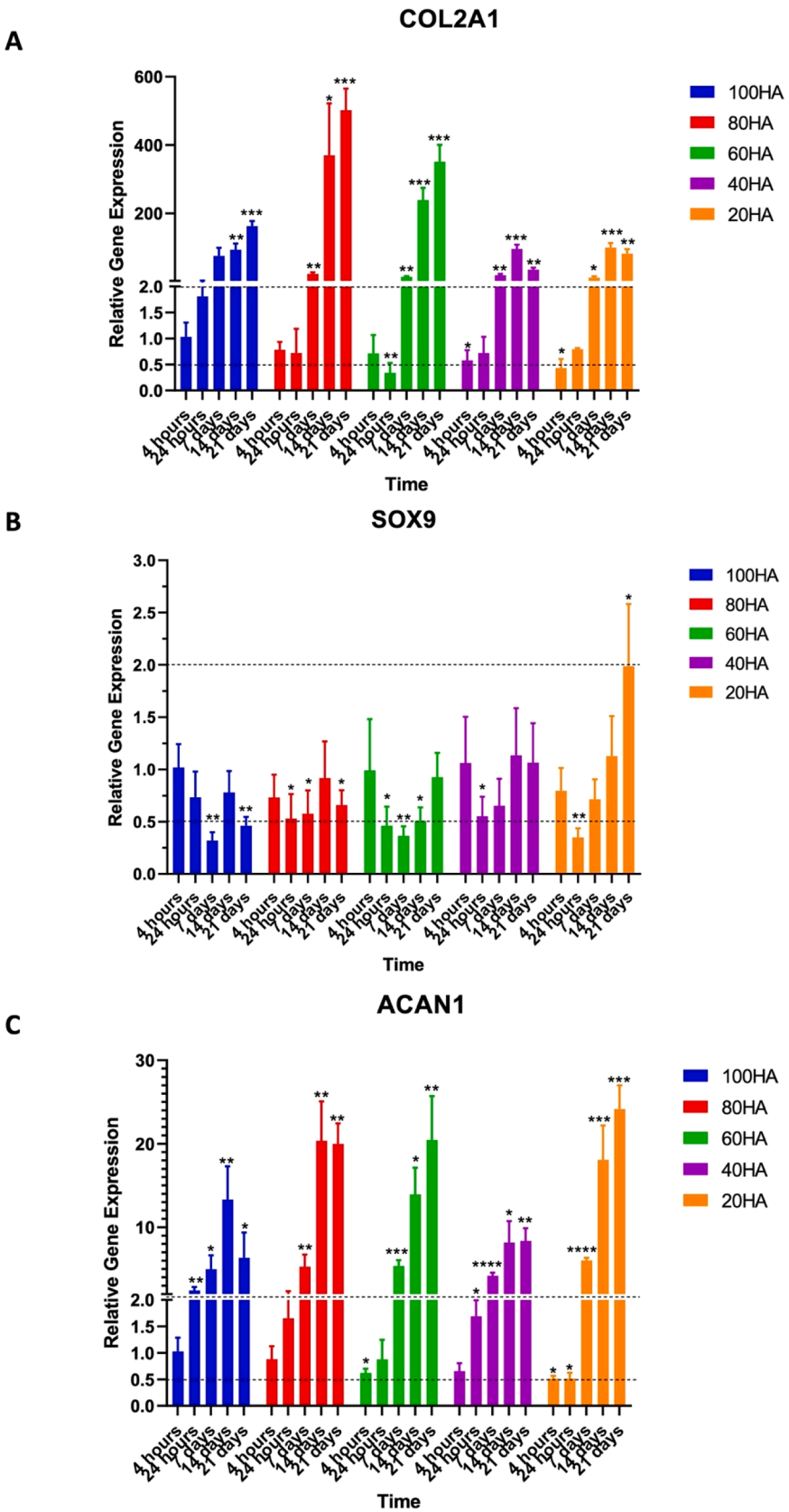

Fig. 6. Chondrogenic potential of NCHA bioinks. A-C) Gene expression profiles over 21 days are displayed showing the mean values of 3 biological repeats presented with standard error, relative to 100HA at 4 h. Dotted lines indicate thresholds of biological significance (<0.5-fold and >2-fold). A) Relative gene expression of COL2A1 demonstrating biologically and statistically significant gene expression in all materials from 7 days relative to 100HA B) Relative gene expression of SOX9 demonstrating biologically and statistically significant increase in gene expression in 20HA relative to 100HA at 21 days. C) Relative gene expression of ACAN1 demonstrating biologically and statistically significant increases in gene expression in all materials from 7 days relative to 100HA.

materials demonstrated superior COL2A1 expression compared to 100HA at 4 h, and this continued to rise for 100HA-60HA, but plateaued at 14–21 days in 40HA and 20HA

SOX9 gene expression was comparable across all materials at 4 h (Fig. 6B). All materials except 100HA then demonstrated a fall in SOX9 expression at 24 h, the sharpest of which was observed in 20HA (0.35, $p = 0.006$). SOX9 expression remained low in 100HA (0.32, $p = 0.005$), 80HA (0.55, $p = 0.031$) and 60HA (0.36, $p = 0.006$) at the 7-day time point, relative to 100HA at 4 h. At 21 days, 60HA and 40HA gene expression had risen to approximately 1, comparable to baseline values in 100HA However, SOX9 expression remained lowered in 100HA (0.46, $p = 0.009$) and 80HA (0.65, $p = 0.04$) at 21 days. The only point at which there was a significant increase in SOX9 expression was in 20HA relative to 100HA (1.99-fold increase, $p = 0.04$).

Aggrecan gene expression (Fig. 6C) was initially lowest in the 60HA (0.6, $p = 0.048$) and 20HA (0.5, $p = 0.03$) bioinks for the first 4 h of culture and this remained significantly reduced for up to 24 h in culture for 20HA (0.5, $p = 0.02$). However, by 7 days of culture, the aggrecan gene expression had risen significantly in all materials, with the most significant rises observed in the 20HA (6.06, $p < 0.0001$) and 40HA (4.20, $p < 0.0001$) materials. Aggrecan gene expression continued to rise over the 21-day course in all biomaterials (except 100HA which subsequently fell at 21 days (6.36, $p = 0.04$) and the highest level was seen at 21 days in the 20HA material (24.16, $p = 0.0004$).

Extracellular matrix production

The extracellular matrix production in each biomaterial was assessed at 21 days using a hydroxyproline assay for collagen content (Fig. 7A) and DMMB assay for sulphated glycosaminoglycan content (Fig. 7B). Mean hydroxyproline content was highest in the 20HA (24.3 ng/ml) and 40HA (24.1 ng/ml) materials: a level that was significantly higher than both 80HA (17.5 ng/ml; $p < 0.0001$) and 100HA (19.8 ng/ml vs 40HA $p = 0.002$, vs 20HA $p = 0.002$). No significant differences were noted between 60HA, 40HA and 20HA

Mean glycosaminoglycan content displayed a similar trend (Fig. 7B), in which content was highest in the 20HA (427.6 μg/ml) and 40HA (430.2 μg/ml) materials relative to 100HA (183.3 μg/ml, $p < 0.0001$), 80HA (259.8 μg/ml, $p = 0.002$) and in this case also 60HA (230.4 μg/ml, $p = 0.0001$). No significant differences were observed between the 40HA and 20HA materials, or between 60HA, 80HA and 100HA

As such, the levels of cartilage extracellular matrix components mirrors the pattern of gene expression: 20HA and 40HA are similarly the most chondrogenic formulations of this bioink.

Toluidine Blue, Alcian Blue and Safranin-O stains were performed to visualise cellular distribution and the presence and arrangement of ECM (Fig. 8). As each material contained some HA, background artefactual staining was anticipated. A violaceous stain was observed in each material stained with Toluidine Blue, particularly around the cells, indicating the cellular deposition of aggrecan. There is evidence of lacunae (less intense pericellular staining) forming around the cells. This is most clearly demonstrated in the 100HA material. Alcian blue stained all biomaterials, with a higher staining density in the pericellular locations and this is particularly well demonstrated in the 20HA, 60HA and 80HA images. Similar pericellular staining was observed with Safranin O, and evidence of cell clustering in lacunae was observed in the 40HA and 60HA images. Of note, there was no evidence of fast-green staining to indicate mineralisation.

Translational suitability of 3D printing human nasoseptal chondrocytes in NCHA bioinks

To determine whether 20HA could be suitably used to produce a complex anatomical, the bioink was used to print a construct representative of a human auricle compared to the same auricle printed in poly-l-lactic acid (PLA) as a control. The 20HA was extrudable and able to reproduce a human auricle with satisfactory fidelity and resolution (Fig. 9B) compared to the PLA control (Fig. 9A). This resolution could not be achieved with HA alone.

The toxicity profile of the 20HA with cells was determined immediately using an LDH assay as a marker of cell lysis (Fig. 10A), compared to a control population of cells only and over 21 days using alamarBlue and live-dead assays (Fig. 10B–C). Baseline cytotoxicity on the LDH assay for cells only was 12.7 %, 7.6 % for cells in NCHA and 2.5 % for cells in HA, with the HA cell cytotoxicity being significantly lower than NCHA and cells alone ($p < 0.0001$). The NCHA did not differ significantly from cells alone, indicating there was no significant cell lysis from the NCHA or crosslinking reaction compared to controls (Fig. 10A).

Over the 21 day time period, chondrocytes demonstrated excellent cell viability within both biomaterials, and an increase in cell number was clear across timepoints as indicated in a higher number of live cells in alamarBlue (Fig. 9B) and live-dead assays (coloured in green Fig. 9C). Significant increases in metabolic activity were seen across all seeding denisities between 0 and 21 days. A sharper increase in metabolic activity was observed in the 500,000 cells between 0 (13.2 %) and 7 (21.1 %) days ($p = 0.019$) which was not observed in the other seeding densities. The highest levels were seen in the 300,000 (37.4 %) and 500,000 (36.9 %) seeded biomaterials at 21 days and statistically similar ($p > 0.999$), but significantly higher than 50,000 cells (<0.0001 vs 300,000 cells; 0.003 vs 500,000 cells).

In the 20HA, cells appeared to form clusters at 21 days indicating proliferation and communication of cells within this biomaterial (Fig. 10C).

In addition to demonstrating the ability to promote *de novo* cartilage, formation, the NCHA bioink (20HA) has additionally demonstrated the ability to be printable and crosslinkable in the shape of the intended anatomical construct without detriment to cell viability, and with evidence of cell proliferation over 21 days. Moreover, the bioinks demonstrated structural stability throughout the 21-day culture period, with no statistically significant differences noted in break force between immediately crosslinked materials and those cultured in media for 21 days with cells (Supplementary Figure 1). This suggests minimal degradation of the nanocellulose component during the study period, and is instrumental for long-term structural stability.

Discussion

This study aimed to develop a biological ink comprised of NC and HA, capable of serving both the biological and mechanical needs of a bespoke facial cartilaginous replacement. We have demonstrated that this biomaterial combination offers excellent printability, mechanical stability and a chondrogenic potential, holding tremendous promise for the future of cartilage bioprinting.

NC augments the printability of HA bioinks

Rheology provides important information about the bioinks in terms of their shear thinning, crosslinking dynamics and ultimately printability. Each HA and NCHA bioink demonstrated shear thinning behaviour over the range of frequencies studied. This is especially important in the context of extrusion-based 3D bioprinting as it means that under the pressure of the extrusion mechanism (usually air), the hydrogel viscosity drops sufficiently to enable the hydrogel to flow through the printer nozzle (Smith et al., 2018).

The viscoelastic properties of the bioinks are also of paramount importance: influencing filament extrusion and fidelity for printing (Petta et al., 2020a). Previous studies have indicated a loss tangent of 0.4–0.6 were ideal for maximum shape fidelity (Petta et al., 2018a, 2018b), which is in the region of the 60–20HA bioinks in this study but considerably lower than the 80HA and 100HA that had loss tangents in excess of 1 for the range of frequencies studied. The bioink formulations with higher NC content therefore, had a dominance of the storage modulus over the loss modulus, which translated to greater elasticity and superior post-printing shape fidelity compared to those with a

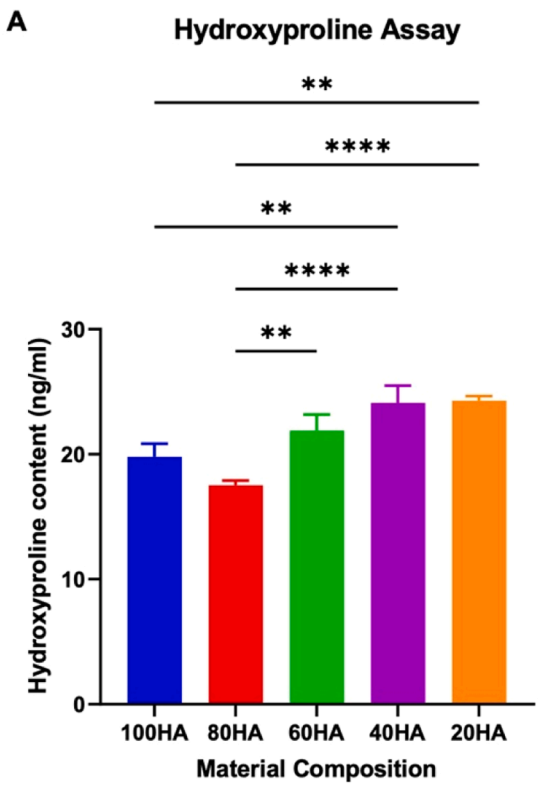

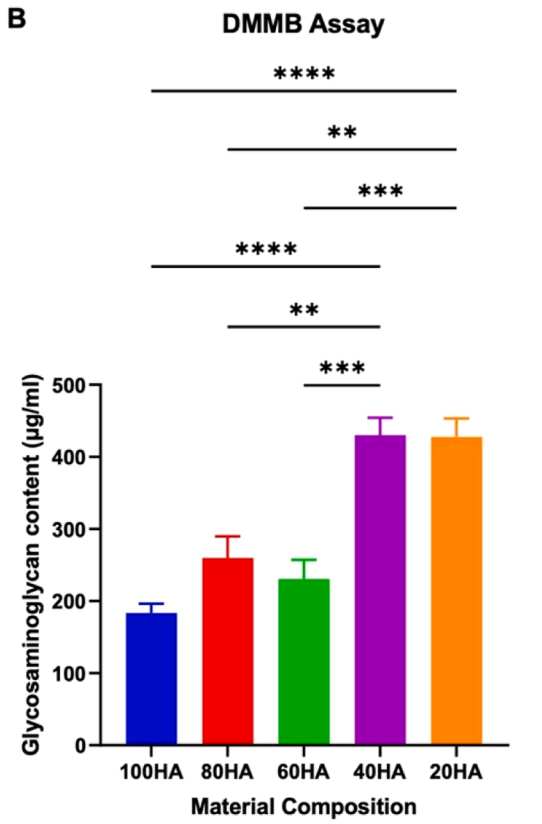

(caption on next column)

Fig. 7. A) The mean levels of hydroxyproline of three biological repeats conducted in technical triplicates is presented with standard deviation. 20HA and 40HA demonstrate statistically significant increases in collagen content compared to 100HA and 80HA B) Dimethylmethylene Blue assay in which the mean of three biological repeats conducted in technical triplicates is presented with standard deviation. 20HA and 40HA demonstrate statistically greater levels of sulphated glycosaminoglycans than 100HA, 80HA and 60HA *=$p < 0.05$; **=$p < 0.01$; ***=$p < 0.001$; ****=$p < 0.0001$.

dominance of HA.

Post-crosslinking shape fidelity was influenced by discrepancies in the swelling and porosity of different NCHA formulations, with crosslinking-induced contraction in 20–40HA bioinks, and the highest degrees of swelling in 100HA and 20HA Hydrogels containing polyelectrolytes have a tendency to swell more owing to charge repulsion between polymer chains (Holback et al., 2011). This has important considerations for the design of 3D printing constructs and allowing for the anticipated swelling that may occur post-crosslinking. Pore geometry of the nanocelluloses used in this study has been undertaken previously, demonstrating pore sizes

Previous studies have similarly demonstrated that the inclusion of NC into bioinks can enhance the viscosity, elasticity and ultimately the printability of bioinks (Markstedt et al., 2015a; Jessop et al., 2019b; Sonnleitner et al., 2021). With regard to NC and alginate, the inclusion of NFC, NCC and NCB variants each augmented the storage modulus of alginate in the magnitude of approximately 60-fold (Jessop et al., 2019b) which is comparable to the difference in storage modulus between 100HA and 20HA/40HA seen at the lower frequencies in this study. Similarly, Markstedt et al. noted that NC-alginate composite bioinks started to become significantly less viscous at a combination of 60 % NFC and 40 % alginate (3 % w/v), which is also comparable to the rheological findings in this study (Markstedt et al., 2015).

NCHA bioinks can be used to produce stable, viable anatomical constructs

We have demonstrated that stable anatomical constructs could be produced using 3D bioprinting and crosslinked without detriment to chondrocyte viability. The pursuit of a biocompatible crosslinking modality is paramount when cells are used in the biofabrication process, and both UV-mediated and peroxidase-mediated approaches have been described for HA, of which each has the potential for cellular genotoxicity and cytotoxicity post-bioprinting (Khunmanee et al., 2017c). In the instance of UV-mediated crosslinking, light intensities of up to 1390 mW/cm^2 have been required to evoke successful UV mediated crosslinking (Clark et al., 2019), creating concerns for genotoxicity and limitations for clinical implementation. The advantage of hydrogen peroxide-mediated crosslinking is control over strength of the crosslinking agent at a safe, biocompatible dose. Biocompatible doses of hydrogen peroxide have been explored previously for cartilage, and have been deemed to fall in the micromolar concentration range, with evidence of cell damage markers reported at doses as low as 50 µM-100 µM (Asada et al., 2001; Khan et al., 2008; Martin et al., 2005). In other cell lines, the genotoxic effect of hydrogen peroxide is seen at concentrations as low as 7.28 µM, emphasising the importance of discovering a 'tolerance threshold' (Seager et al., 2012) for cellular viability, but ensuring adequate crosslinking strength for post-printing shape fidelity. In our study, the cytotoxic threshold of human nasoseptal chondrocytes was between 10 and 20 µM, however even doses of 5 µM were capable of adequately crosslinking the NCHA, as demonstrated by comparable elastic moduli, swelling and compressive strength relative to 115 mM. Rheologically, it was demonstrated that adequate crosslinking could be achieved within 5 to 10 min, enabling the production of convincing anatomical constructs to be created using extrusion 3D bioprinting.

Importantly, all cells encapsulated in the bioinks demonstrated evidence of increasing cell number and good viability over the course of 21 days in culture. Furthermore, cells embedded in the NCHA exposed to

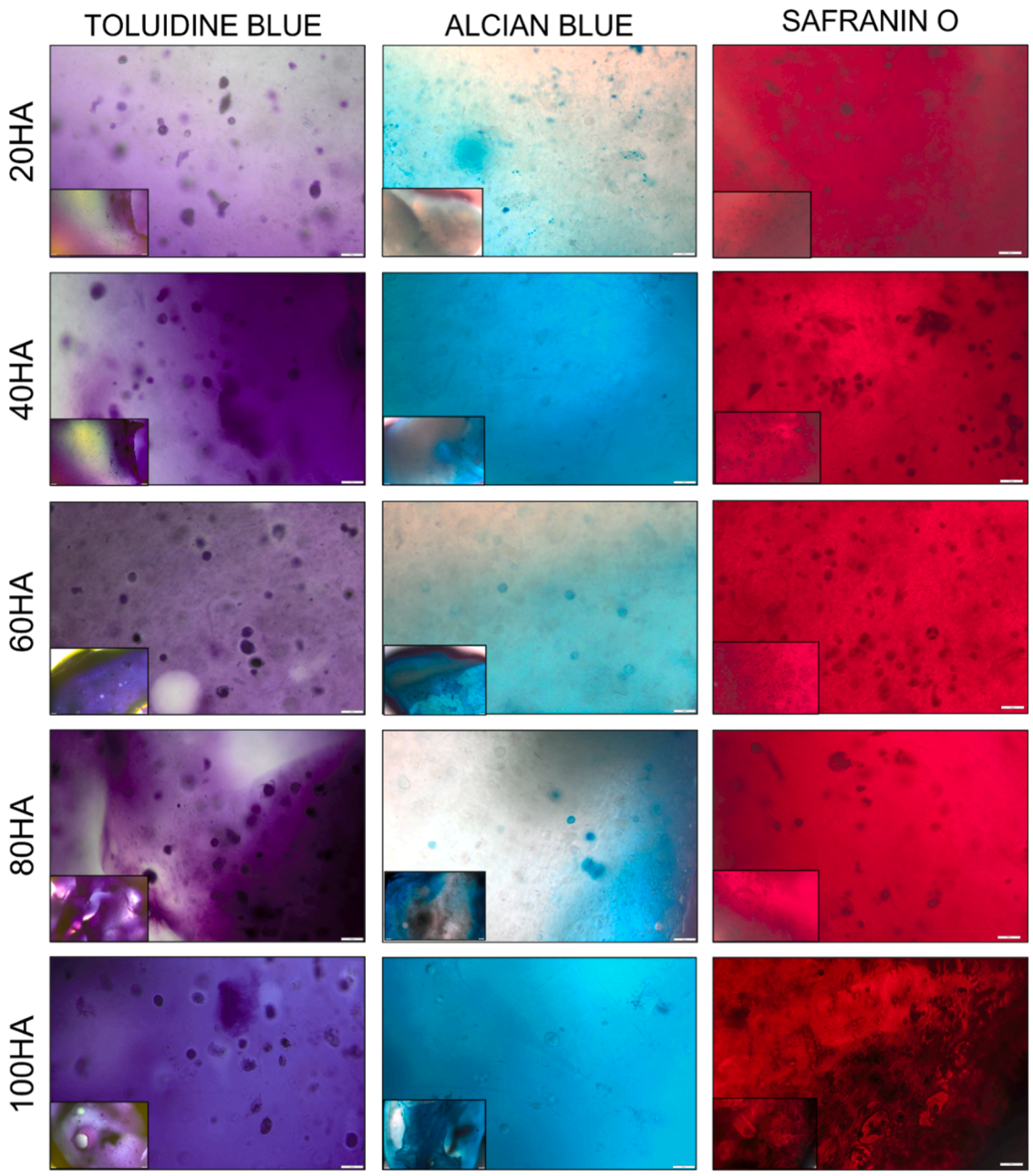

Fig. 8. Histological stains for extracellular matrix in intact NCHA bioinks. Each material is presented at 4x (small image) and 20x (large image) magnification stained with Toluidine Blue (left) and Alcian Blue (middle) and Safranin O (right). Intense uptake of stains is seen in a pericellular location in all biomaterials, indicative of extracellular matrix production. The cells can also be seen to be forming lacunae in a number of the stained specimens. Scale bars (bottom right of the 20x magnification images) depict 50 μm.

the low dose (5 μM) hydrogen peroxide crosslinking agent appeared to have minimal cytotoxicity. HA generally is perceived to have good biocompatibility: enhanced cell viability and proliferation have been observed in other studies when added as a third constituent to NC-alginate inks (Lafuente-Merchan et al., 2021). Similarly viability benefits have been previously reported when culturing adipocytes in HA, where an immediate viability of 64 % increased to 95 % at 7 days of culture (Henriksson et al., 2017). These findings support HA an ideal bioink constituent for cartilage bioprinting, both from a printability perspective but moreover as a biomaterial with excellent biocompatibility and biomimicry. NC itself has also been demonstrated to possess excellent biocompatibility: successfully supporting cell growth and viability both in vitro and in vivo with multiple cell and tissue types (Apelgren et al., 2019; Halib et al., 2017; Jovic et al., 2019b, 2023b; Kumar et al., 2024).

NCHA bioinks support de novo cartilage formation

Plant-derived NC has been previously demonstrated to augment the printability and chondrogenicity of alginate (Jessop, Al-Sabah et al., 2019a; Jovic et al., 2023a; Martínez Ávila et al., 2016). In this study, we refine the optimum combinations of a novel NCB formulation comprising both crystalline and fibrillar components with a cross-linkable HA, to demonstrate high levels of chondrogenic potential with primary human nasoseptal chondrocytes.

All combinations demonstrated an inherent chondrogenic potential as evidenced by rising relative gene expression of ACAN and COL2A1 over the course of 21 days, indicating the NC and HA materials produce

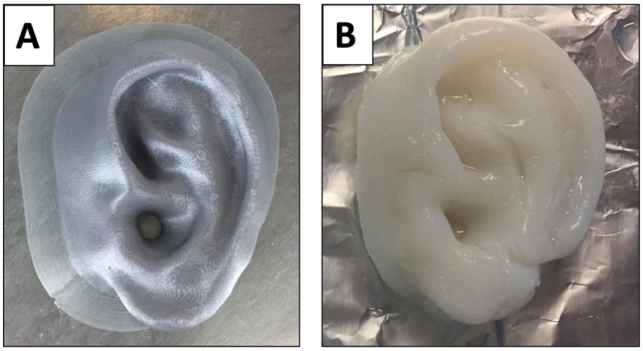

Fig. 9. A-B) Digital photographs of human auricles printed in A) Polylactic acid (using an Ultimaker 3 Printer) as a control B) 20HA crosslinked with 5 μM printed using the CELLINK INKREDIBLE printer. HA was unsuccessfully printed (not shown).

an environment conducive of extracellular matrix formation. This was supported at the level of extracellular matrix content, where collagen (hydroxyproline) and non-sulphated glycosaminoglycans were detectible in all material combinations. There was a trend observed at the 21-day time point indicating that the 40HA and 20HA materials evoked the greatest response in chondrogenic, extracellular matrix gene expression (COL2A1 and ACAN), which aligns to these materials having the greatest hydroxyproline and non-sulphated GAG content at 21 days. These two molecules are key components of nasoseptal cartilage extracellular matrix (Jessop, Zhang et al., 2019) and to have a sustained elevation of their gene expression indicates that appropriate environmental cues are being provided for sustained cartilage formation. NFC and NCC are believed to have structural mimicry to collagen fibres and extracellular matrix ground substance respectively, which may contribute to the augmented gene expression profiles observed.

SOX9 gene expression rose most significantly in the 20HA material, which as an upstream mediator of chondrogenicity, secures differentiation down a chondrocytic lineage, promotes cell survival and is a transcriptional activator of COL2A1 and ACAN (Lefebvre & Dvir-Ginzberg, 2017). As such, this chronological effect seen in the 21-day PCR data reflects a recognised gene expression sequence (Bar Oz et al., 2016), however the effect is believed to have the potential to be bidirectional, with overexpression of SOX9 causing an attenuation of COL2A1 expression (Kypriotou et al., 2003).

Combined, the histological evidence, with gene expression and ECM production, indicates that these materials offer a suitable mimicry of the chondrogenic milieu for bioengineering purposes.

The ability of cells to migrate within the NCHA bioink may have advantageous effects for biomimicry, enabling cells to adopt a round morphology and exist in lacunae of single cells or a small cluster of cells, surrounded by dense pericellular matrix, as visualised on histological analysis. This is part is attributable to its microarchitecture, with the NCB formulation used in this bioink comprising pore sizes of ranging between 55 and 1200 nm (mean 934 nm). Pores in the nano-scale (<100 nm) play important roles in facilitating ECM and collagen production, whereas macropores (100um-1 mm) play important roles in cell distribution and migration (Bružauskaitė et al., 2016). The NCB formulation exhibits a high range of pore sizes spanning from 55 nm to 12 μm, meaning it falls primarily into the nano- and microporosity range of pore sizes, facilitating ECM deposition and cell migration respectively (Bružauskaitė et al., 2016; Kyle et al., 2018b). We have previously demonstrated, NCB facilitates good cell integration within the pores visualised with scanning electron microscopy (SEM) imaging, with a large variation in pore sizes primarily in the micro and nano range providing a larger area for cell adhesion (Supplementary Figure 2) (Al-Sabah et al., 2019b; Jessop, Al-Sabah et al., 2019b). This highly biocompatible and bioactive combination of HA and NC therefore holds promise for future clinical applications.

Furthermore, the NC component is non-degradable in humans owing to an absence of cellulase enzymes, conferring structural stability and longevity confirmed during this 21-day time period with mechanical testing. The degradable HA component however, has demonstrated an affinity to promote chondrogenesis, enabling progressive replacement of the HA scaffold with cartilage ECM, with degradation postulated to occur within months (Wang et al., 2022). Further in vivo verification of the degradation and repopulation profile will be required prior to clinical implementation.

Conclusion

NC has a proven record of excellent printability and chondrogenicity properties. It holds tremendous promise for bioprinting cartilage tissue, augmented further by the addition of hyaluronic acid as a chondrogenic and biocompatible additive. This material blend is readily printable into complex anatomical structures including human auricles, and promotes the expansion and differentiation of chondrocytes to encourage the formation of tissue that mimics native cartilage tissue. Chondrocytes thrived in all HA, and NCHA biomaterials studied, showing sustained increases in chondrogenic gene expression and increases in cell number over 21 days, rendering them each valid biomaterials for cartilage tissue engineering. It is apparent that bioinks with higher percentages of NC (20HA and 40HA) possess superior rheological, structural and chondrogenic properties but that replacing the alginate with hyaluronic acid augments the chondrogenicity of the bioink. These features, combined with its excellent printability, make NCHA an incredibly promising biomaterial for 3D bioprinting facial cartilages.

Data availability statement:

The datasets generated and analysed during the current study are available from the corresponding author on reasonable request. Data pertaining to the demographics of the patient samples used in this study are not publicly available in line with our ethical approval.

Funding

This study was supported by The Scar Free Foundation & Health and Care Research Wales Programme of research in Reconstructive Surgery & Regenerative Medicine, which has been established in the ReconRegen Research Centre at Swansea University in partnership with Swansea Bay University Health Board.

Additionally, THJ would like to acknowledge funding from Action Medical Research and the VTCT Foundation (GN2782), Microtia UK, the Royal College of Surgeons England, the British Association of Plastic and Reconstructive Surgeons and the Welsh Clinical Academic Training Programme.

Conflicts of Interest: ISW would like to disclose a previously submitted patent application for the development of nanocellulose bioinks (Patent Pending: US16/976,803).

Ethics approval

Human cells used in this study were acquired with, and used in line with, ethical approval and informed patient consent under the study title "Collection of Surgical Biopsies for Regenerative Medicine and Related Research", granted June 2015 (Research Ethics Committee, National Institute for Social Care and Health Research, Welsh Government, IRAS ID 99,202).

Patient consent statement

All human tissues acquired in this study were acquired with informed patient consent in line with our ethical approval statement

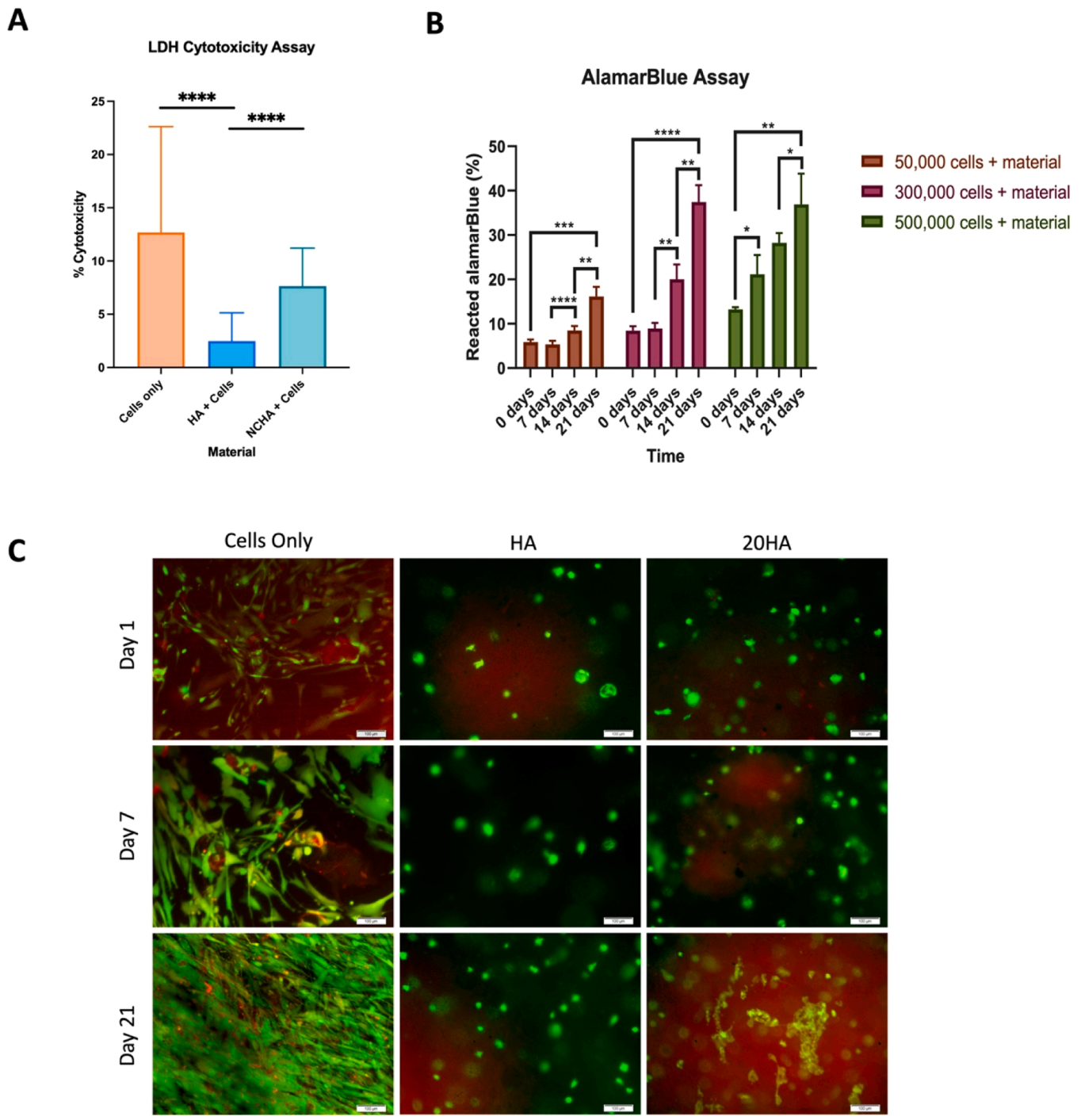

Fig. 10. A) LDH Cytotoxicity assay of cells in biomaterials taken at 4 h. Mean values from 9 repeats are presented with standard deviation. Statistical analysis from a one-way ANOVA is presented, with cells only (not embedded within a biomaterial) presented for reference. B) AlamarBlue assay of different seeding densities in 20HA bioink acquired at day 0, 7, 14 and 21 across three seeding densities (50,000; 300,000 and 500,000 cells per 100 μl biomaterial). Increases in metabolic activity cell number were observed in all biomaterials. Mean values of 6 replicates are presented with standard deviation. Results from a one-way ANOVA and Tukey's post hoc test are presented. C) Live dead assay of candidate biomaterials at Day 1 (top row), Day 7 (middle row) and Day 21 (bottom row) of culture containing human nasoseptal chondrocytes for HA and 20HA Materials are compared to 'cells only' (left column) for each time point. Morphologically the cells maintained a rounded appearance in the 3D culture conditions relative to cell only conditions and appear to have fewer dead cell signals detectable at each time point. Live cells are stained with Calcein AM, detected on the FITC channel and coloured green in these images, whereas dead cells stained with Ethidium homodimer were detected on the TRITC channel and have been coloured red for illustrative purposes. All images are acquired at 20x magnification with scale bars depicting 100 μm. *=$p < 0.05$, **=$p < 0.01$; ***=$p < 0.001$; ****=$p < 0.0001$.

CRediT authorship contribution statement

Thomas H Jovic: Writing – original draft, Visualization, Methodology, Investigation, Funding acquisition, Formal analysis, Data curation, Conceptualization. **Andrea Gazze:** Writing – original draft, Software, Methodology, Investigation, Formal analysis. **Bethan Morgan:** Methodology, Investigation, Formal analysis, Data curation. **Karl Hawkins:** Validation, Supervision, Software, Methodology,

Investigation. **Lewis Francis:** Writing – review & editing, Supervision, Software, Resources, Methodology, Investigation. **Hari Arora:** Writing – review & editing, Validation, Software, Resources, Methodology, Investigation. **Shareen H Doak:** Writing – review & editing, Validation, Supervision, Resources, Project administration, Methodology, Investigation, Conceptualization. **Iain S Whitaker:** Writing – review & editing, Validation, Supervision, Software, Resources, Methodology, Investigation, Conceptualization.

Declaration of competing interest

The authors declare the following financial interests/personal relationships which may be considered as potential competing interests: ISW would like to disclose a previously submitted patent application for the development of nanocellulose bioinks (Patent Pending: US16/976,803).

Acknowledgements

The authors would like to acknowledge the support of AVAPCO for supplying the nanocelluloses and Ms Kavitha Saw for supplying the nasoseptal cartilage samples for chondrocytes used in this study.

Supplementary materials

Supplementary material associated with this article can be found, in the online version, at doi:10.1016/j.carpta.2025.100929.

Data availability

Data will be made available on request.

References

Al-Himdani, S., Jessop, Z. M., Al-Sabah, A., Combellack, E., Ibrahim, A., Doak, S. H., Hart, A. M., Archer, C. W., Thornton, C. A., & Whitaker, I. S. (2017). Tissue-engineered solutions in plastic and reconstructive surgery: Principles and practice. *Frontiers in Surgery, 4*(4). https://doi.org/10.3389/fsurg.2017.00004

Al-Sabah, A., Burnell, S. E. A., Simoes, I. N., Jessop, Z., Badiei, N., Blain, E., & Whitaker, I. S. (2019a). Structural and mechanical characterization of crosslinked and sterilised nanocellulose-based hydrogels for cartilage tissue engineering. *Carbohydrate Polymers, 212*, 242–251. https://doi.org/10.1016/j.carbpol.2019.02.057

Al-Sabah, A., Burnell, S. E. A., Simoes, I. N., Jessop, Z., Badiei, N., Blain, E., & Whitaker, I. S. (2019b). Structural and mechanical characterization of crosslinked and sterilised nanocellulose-based hydrogels for cartilage tissue engineering. *Carbohydrate Polymers, 212*, 242–251. https://doi.org/10.1016/j.carbpol.2019.02.057

Apelgren, P., Amoroso, M., Lindahl, A., Brantsing, C., Rotter, N., Gatenholm, P., & Kölby, L. (2017). Chondrocytes and stem cells in 3D-bioprinted structures create human cartilage in vivo. *PloS One*, (12), 12. https://doi.org/10.1371/JOURNAL.PONE.0189428

Apelgren, P., Karabulut, E., Amoroso, M., Mantas, A., Martínez Ávila, H., Kölby, L., Kondo, T., Toriz, G., & Gatenholm, P. (2019). In vivo Human cartilage formation in three-dimensional bioprinted constructs with a novel bacterial nanocellulose bioink. *ACS Biomaterials Science and Engineering, 5*(5), 2482–2490. https://doi.org/10.1021/ACSBIOMATERIALS.9B00157/ASSET/IMAGES/LARGE/AB-2019-00157T_0002.JPEG

Asada, S., Fukuda, K., Nishisaka, F., Matsukawa, M., & Hamanisi, C. (2001). Hydrogen peroxide induces apoptosis of chondrocytes; involvement of calcium ion and extracellular signal-regulated protein kinase. *Inflammation Research 2001 50:1, 50* (1), 19–23. https://doi.org/10.1007/S000110050719

Bar Oz, M., Kumar, A., Elayyan, J., Reich, E., Binyamin, M., Kandel, L., Liebergall, M., Steinmeyer, J., Lefebvre, V., & Dvir-Ginzberg, M. (2016). Acetylation reduces SOX9 nuclear entry and ACAN gene transactivation in human chondrocytes. *Aging Cell, 15* (3), 499. https://doi.org/10.1111/ACEL.12456

Bružauskaitė, I., Bironaitė, D., Bagdonas, E., & Bernotienė, E. (2016). Scaffolds and cells for tissue regeneration: Different scaffold pore sizes—Different cell effects. *Cytotechnology, 68*(3), 355. https://doi.org/10.1007/S10616-015-9895-4

Clark, C. C., Aleman, J., Mutkus, L., & Skardal, A. (2019). A mechanically robust thixotropic collagen and hyaluronic acid bioink supplemented with gelatin nanoparticles. *Bioprinting, 16*, Article e00058. https://doi.org/10.1016/J.BPRINT.2019.E00058

Cooper, C., Rannou, F., Richette, P., Bruyère, O., Al-Daghri, N., Altman, R. D., Brandi, M. L., Collaud Basset, S., Herrero-Beaumont, G., Migliore, A., Pavelka, K., Uebelhart, D., & Reginster, J. Y. (2017). Use of intraarticular hyaluronic acid in the management of knee osteoarthritis in clinical practice. *Arthritis Care & Research, 69* (9), 1287–1296. https://doi.org/10.1002/ACR.23204

Fagien, S., Bertucci, V., von Grote, E., & Mashburn, J. H. (2019). Rheologic and physicochemical properties used to differentiate injectable hyaluronic acid filler products. *Plastic and Reconstructive Surgery, 143*(4). https://doi.org/10.1097/PRS.0000000000005429, 707e–720e.

Fallacara, A., Baldini, E., Manfredini, S., & Vertuani, S. (2018). Hyaluronic acid in the third millennium. *Polymers*, (7), 10. https://doi.org/10.3390/POLYM10070701

Graça, M. F. P., Miguel, S. P., Cabral, C. S. D., & Correia, I. J. (2020). Hyaluronic acid-based wound dressings: A review. *Carbohydrate Polymers*, 241. https://doi.org/10.1016/J.CARBPOL.2020.116364

Gupta, R. C., Lall, R., Srivastava, A., & Sinha, A. (2019). Hyaluronic acid: Molecular mechanisms and therapeutic trajectory. *Frontiers in Veterinary Science, 6*, 192. https://doi.org/10.3389/FVETS.2019.00192 (JUN).

Halib, N., Perrone, F., Cemazar, M., Dapas, B., Farra, R., Abrami, M., Chiarappa, G., Forte, G., Zanconati, F., Pozzato, G., Murena, L., Fiotti, N., Lapasin, R., Cansolino, L., Grassi, G., & Grassi, M. (2017). Potential applications of nanocellulose-containing materials in the biomedical field. *Materials, 10*(8), 977. https://doi.org/10.3390/ma10080977

Hauptstein, J., Böck, T., Bartolf-Kopp, M., Forster, L., Stahlhut, P., Nadernezhad, A., Blahetek, G., Zernecke-Madsen, A., Detsch, R., Jüngst, T., Groll, J., Teßmar, J., & Blunk, T. (2020). Hyaluronic acid-based bioink composition enabling 3D bioprinting and improving quality of deposited cartilaginous extracellular matrix. *Advanced Healthcare Materials, 9*(15), Article 2000737. https://doi.org/10.1002/ADHM.202000737

Heid, S., & Boccaccini, A. R. (2020). Advancing bioinks for 3D bioprinting using reactive fillers: A review. *Acta Biomaterialia, 113*, 1–22. https://doi.org/10.1016/J.ACTBIO.2020.06.040

Henriksson, I., Gatenholm, P., & Hägg, D. A. (2017). Increased lipid accumulation and adipogenic gene expression of adipocytes in 3D bioprinted nanocellulose scaffolds. *Biofabrication, 9*(1), Article 015022. https://doi.org/10.1088/1758-5090/aa5c1c

Holback, H., Yeo, Y., & Park, K. (2011). Hydrogel swelling behavior and its biomedical applications. *Biomedical Hydrogels*, 3–24. https://doi.org/10.1533/9780857091383.1.3

Jessop, Z.M., Al-Himdani, S., Clement, M., & Whitaker, I.S. (2015). The challenge for reconstructive surgeons in the twenty-First century: Manufacturing tissue-engineered solutions. In *Frontiers in Surgery* (Vol. 2, p. 52). https://doi.org/10.3389/fsurg.2015.00052.

Jessop, Z. M., Al-Sabah, A., Francis, W. R., & Whitaker, I. S. (2016a). Transforming healthcare through regenerative medicine. *BMC Medicine, 14*(1), 115. https://doi.org/10.1186/s12916-016-0669-4

Jessop, Z. M., Al-Sabah, A., Gao, N., Kyle, S., Thomas, B., Badiei, N., Hawkins, K., & Whitaker, I. S. (2019a). Printability of pulp derived crystal, fibril and blend nanocellulose-alginate bioinks for extrusion 3D bioprinting. *Biofabrication, 11*(4), Article 045006. https://doi.org/10.1088/1758-5090/ab0631

Jessop, Z. M., Al-Sabah, A., Gao, N., Kyle, S., Thomas, B., Badiei, N., Hawkins, K., & Whitaker, I. S. (2019b). Printability of pulp derived crystal, fibril and blend nanocellulose-alginate bioinks for extrusion 3D bioprinting. *Biofabrication, 11*(4), Article 045006. https://doi.org/10.1088/1758-5090/ab0631

Jessop, Z. M., Javed, M., Otto, I. A., Combellack, E. J., Morgan, S., Breugem, C. C., Archer, C. W., Khan, I. M., Lineaweaver, W. C., Kon, M., Malda, J., & Whitaker, I. S. (2016b). Combining regenerative medicine strategies to provide durable reconstructive options: Auricular cartilage tissue engineering. *Stem Cell Research & Therapy, 7*(1), 19. https://doi.org/10.1186/s13287-015-0273-0

Jessop, Z. M., Zhang, Y., Simoes, I., Al-Sabah, A., Badiei, N., Gazze, S. A., Francis, L., & Whitaker, I. S. (2019). Morphological and biomechanical characterization of immature and mature nasoseptal cartilage. *Scientific Reports 2019 9:1, 9*(1), 1–12. https://doi.org/10.1038/s41598-019-48578-3

Jovic, T. H., Combellack, E. J., Jessop, Z. M., & Whitaker, I. S. (2020a). 3D Bioprinting and the future of surgery. *Frontiers in Surgery, 7*, Article 609836. https://doi.org/10.3389/fsurg.2020.609836

Jovic, T. H., Combellack, E. J., Jessop, Z. M., & Whitaker, I. S. (2020b). 3D Bioprinting and the future of surgery. *Frontiers in Surgery, 7*, Article 609836. https://doi.org/10.3389/fsurg.2020.609836

Jovic, T. H., Jessop, Z. M., Al-Sabah, A., & Whitaker, I. S. (2018). The clinical need for 3D printed tissue in reconstructive surgery. *3D Bioprinting for Reconstructive Surgery*, 235–244. https://doi.org/10.1016/B978-0-08-101103-4.00002-8

Jovic, T.H., Kungwengwe, G., Mills, A.C., & Whitaker, I.S. (2019a). Plant-derived biomaterials: A review of 3D bioprinting and biomedical applications. In *Frontiers in mechanical engineering* (Vol. 5). Frontiers Media SA. https://doi.org/10.3389/fmech.2019.00019.

Jovic, T.H., Kungwengwe, G., Mills, A.C., & Whitaker, I.S. (2019b). Plant-derived biomaterials: A review of 3D bioprinting and biomedical applications. In *Frontiers in mechanical engineering* (Vol. 5). Frontiers Media SA. https://doi.org/10.3389/fmech.2019.00019.

Jovic, T. H., Nicholson, T., Arora, H., Nelson, K., Doak, S. H., & Whitaker, I. S. (2023a). A comparative analysis of pulp-derived nanocelluloses for 3D bioprinting facial cartilages. *Carbohydrate Polymers*. , Article 121261. https://doi.org/10.1016/J.CARBPOL.2023.121261

Jovic, T. H., Nicholson, T., Arora, H., Nelson, K., Doak, S. H., & Whitaker, I. S. (2023b). A comparative analysis of pulp-derived nanocelluloses for 3D bioprinting facial cartilages. *Carbohydrate Polymers*. , Article 121261. https://doi.org/10.1016/J.CARBPOL.2023.121261

Khan, I. M., Gilbert, S. J., Caterson, B., Sandell, L. J., & Archer, C. W. (2008). Oxidative stress induces expression of osteoarthritis markers procollagen IIA and 3B3(−) in

adult bovine articular cartilage. *Osteoarthritis and Cartilage, 16*(6), 698–707. https://doi.org/10.1016/J.JOCA.2007.10.004

Khunmanee, S., Jeong, Y., & Park, H. (2017a). Crosslinking method of hyaluronic-based hydrogel for biomedical applications. *Journal of Tissue Engineering, 8*. https://doi.org/10.1177/2041731417726464

Khunmanee, S., Jeong, Y., & Park, H. (2017b). Crosslinking method of hyaluronic-based hydrogel for biomedical applications. *Journal of Tissue Engineering, 8*. https://doi.org/10.1177/2041731417726464

Khunmanee, S., Jeong, Y., & Park, H. (2017c). Crosslinking method of hyaluronic-based hydrogel for biomedical applications. *Journal of Tissue Engineering, 8*. https://doi.org/10.1177/2041731417726464, 2041731417726464.

Kiani, C., Chen, L., Wu, Y. J., Yee, A. J., & Yang, B. B. (2002). Structure and function of aggrecan. *Cell Research 2002 12:1, 12*(1), 19–32. https://doi.org/10.1038/sj.cr.7290106

Kumar, S., Kumar, D., Upadhyay, C., Bansal, M., Rathi, B., & Singh, P. (2024). Functionalization of cellulose nanocrystals with a potent antimalarial compound: Synthesis, characterization, and biological studies. *International Journal of Biological Macromolecules, 282*, Article 136660. https://doi.org/10.1016/J.IJBIOMAC.2024.136660

Kyle, S., Jessop, Z. M., Al-Sabah, A., Hawkins, K., Lewis, A., Maffeis, T., Charbonneau, C., Gazze, A., Francis, L. W., Iakovlev, M., Nelson, K., Eichhorn, S. J., & Whitaker, I. S. (2018a). Characterization of pulp derived nanocellulose hydrogels using AVAP® technology. *Carbohydrate Polymers, 198*, 270–280.

Kyle, S., Jessop, Z. M., Al-Sabah, A., Hawkins, K., Lewis, A., Maffeis, T., Charbonneau, C., Gazze, A., Francis, L. W., Iakovlev, M., Nelson, K., Eichhorn, S. J., & Whitaker, I. S. (2018b). Characterization of pulp derived nanocellulose hydrogels using AVAP® technology. *Carbohydrate Polymers, 198*, 270–280. http://www.ncbi.nlm.nih.gov/pubmed/30093000.

Kypriotou, M., Fossard-Demoor, M., Chadjichristos, C., Ghayor, C., De Crombrugghe, B., Pujol, J. P., & Galéra, P. (2003). SOX9 exerts a bifunctional effect on type II collagen gene (COL2A1) expression in chondrocytes depending on the differentiation state. *DNA and Cell Biology, 22*(2), 119–129. https://doi.org/10.1089/104454903321515922

Lafuente-Merchan, M., Ruiz-Alonso, S., Espona-Noguera, A., Galvez-Martin, P., López-Ruiz, E., Marchal, J. A., López-Donaire, M. L., Zabala, A., Ciriza, J., Saenz-del-Burgo, L., & Pedraz, J. L. (2021). Development, characterization and sterilisation of nanocellulose-alginate-(hyaluronic acid)- bioinks and 3D bioprinted scaffolds for tissue engineering. *Materials Science and Engineering: C, 126*, Article 112160. https://doi.org/10.1016/J.MSEC.2021.112160

Lefebvre, V., & Dvir-Ginzberg, M. (2017). SOX9 and the many facets of its regulation in the chondrocyte lineage. *Connective Tissue Research, 58*(1), 2. https://doi.org/10.1080/03008207.2016.1183667

Livak, K. J., & Schmittgen, T. D. (2001). Analysis of relative gene expression data using real-time quantitative PCR and the 2-ΔΔCT method. *Methods (San Diego, Calif.), 25*(4), 402–408. https://doi.org/10.1006/meth.2001.1262

Malkoc, V. (2018). Challenges and the future of 3D bioprinting. *Journal of Biomedical Imaging and Bioengineering, 1*(3), 62–63. http://www.alliedacademies.org/biomedical-imaging-and-bioengineering/.

Markstedt, K., Mantas, A., Tournier, I., Martínez Ávila, H., Hägg, D., & Gatenholm, P. (2015). 3D bioprinting human chondrocytes with nanocellulose-alginate bioink for cartilage tissue engineering applications. *Biomacromolecules, 16*(5), 1489–1496. https://doi.org/10.1021/acs.biomac.5b00188

Martin, G., Andriamanalijaona, R., Mathy-Hartert, M., Henrotin, Y., & Pujol, J. P. (2005). Comparative effects of IL-1β and hydrogen peroxide (H2O2) on catabolic and anabolic gene expression in juvenile bovine chondrocytes. *Osteoarthritis and Cartilage, 13*(10), 915–924. https://doi.org/10.1016/J.JOCA.2005.03.009

Martínez Ávila, H., Schwarz, S., Rotter, N., & Gatenholm, P. (2016). 3D bioprinting of human chondrocyte-laden nanocellulose hydrogels for patient-specific auricular cartilage regeneration. *Bioprinting*, (1–2), 22–35. https://doi.org/10.1016/J.BPRINT.2016.08.003

Möller, T., Amoroso, M., Hägg, D., Brantsing, C., Rotter, N., Apelgren, P., Lindahl, A., Kölby, L., & Gatenholm, P. (2017). In vivo chondrogenesis in 3D bioprinted Human cell-laden hydrogel constructs. *Plastic and Reconstructive Surgery - Global Open, 5*(2), e1227. https://doi.org/10.1097/GOX.0000000000001227

Müller, M., Öztürk, E., Arlov, Ø., Gatenholm, P., & Zenobi-Wong, M. (2017). Alginate sulfate–Nanocellulose bioinks for cartilage bioprinting applications. *Annals of Biomedical Engineering, 45*(1), 210–223. https://doi.org/10.1007/s10439-016-1704-5

Nelson, K., & Restina, T. (2014). Innovative nanocellulose process breaks the cost barrier. *TAPPI Journal, 13*(5), 19–23. https://doi.org/10.32964/TJ13.5.19

Petta, D., Armiento, A. R., Grijpma, D., Alini, M., Eglin, D., & D'Este, M. (2018). 3D bioprinting of a hyaluronan bioink through enzymatic-and visible light-crosslinking. *Biofabrication, 10*(4), Article 044104. https://doi.org/10.1088/1758-5090/AADF58

Petta, D., Grijpma, D. W., Alini, M., Eglin, D., & D'Este, M. (2018a). Three-dimensional printing of a tyramine hyaluronan derivative with double gelation mechanism for independent tuning of shear thinning and postprinting curing. *ACS Biomaterials Science and Engineering, 4*(8), 3088–3098. https://doi.org/10.1021/ACSBIOMATERIALS.8B00416/SUPPL_FILE/AB8B00416_SI_007.PDF

Petta, D., Grijpma, D. W., Alini, M., Eglin, D., & D'Este, M. (2018b). Three-dimensional printing of a tyramine hyaluronan derivative with double gelation mechanism for independent tuning of shear thinning and postprinting curing. *ACS Biomaterials Science and Engineering, 4*(8), 3088–3098. https://doi.org/10.1021/ACSBIOMATERIALS.8B00416/SUPPL_FILE/AB8B00416_SI_007.PDF

Petta, D., Petta, D., D'Amora, U., Ambrosio, L., Grijpma, D. W., Eglin, D., Eglin, D., & D'Este, M. (2020a). Hyaluronic acid as a bioink for extrusion-based 3D printing. *Biofabrication, 12*(3), Article 032001. https://doi.org/10.1088/1758-5090/AB8752

Petta, D., Petta, D., D'Amora, U., Ambrosio, L., Grijpma, D. W., Eglin, D., Eglin, D., & D'Este, M. (2020b). Hyaluronic acid as a bioink for extrusion-based 3D printing. *Biofabrication, 12*(3), Article 032001. https://doi.org/10.1088/1758-5090/AB8752

Poldervaart, M. T., Goversen, B., De Ruijter, M., Abbadessa, A., Melchels, F. P. W., Öner, F. C., Dhert, W. J. A., Vermonden, T., & Alblas, J. (2017). 3D bioprinting of methacrylated hyaluronic acid (MeHA) hydrogel with intrinsic osteogenicity. *PLOS ONE, 12*(6), Article e0177628. https://doi.org/10.1371/JOURNAL.PONE.0177628

Seager, A. L., Shah, U.-K., Mikhail, J. M., Nelson, B. C., Marquis, B. J., Doak, S. H., Johnson, G. E., Griffiths, S. M., Carmichael, P. L., Scott, S. J., Scott, A. D., & Jenkins, G. J. S. (2012). Pro-oxidant induced DNA damage in Human lymphoblastoid cells: Homeostatic mechanisms of genotoxic tolerance. *Toxicological Sciences, 128*(2), 387–397. https://doi.org/10.1093/toxsci/kfs152

Smith, P. T., Basu, A., Saha, A., & Nelson, A. (2018). Chemical modification and printability of shear-thinning hydrogel inks for direct-write 3D printing. *Polymer, 152*, 42–50. https://doi.org/10.1016/J.POLYMER.2018.01.070

Sonnleitner, D., Schrüfer, S., Berglund, L., Schubert, D. W., & Lang, G. (2021). Correlating rheology and printing performance of fiber-reinforced bioinks to assess predictive modelling for biofabrication. *Journal of Materials Research, 36*(19), 3821–3832. https://doi.org/10.1557/S43578-021-00276-5/FIGURES/7

Tarassoli, S. P., Jessop, Z. M., Jovic, T., Hawkins, K., & Whitaker, I. S. (2021). Candidate bioinks for extrusion 3D bioprinting—A systematic review of the literature. *Frontiers in Bioengineering and Biotechnology, 0*, 383. https://doi.org/10.3389/FBIOE.2021.616753

Truong, T., & Maricevich, R. (2017). Ear reconstruction. *Seminars in Plastic Surgery, 31*(03), 125–126. https://doi.org/10.1055/s-0037-1604242

Vincent, T. L., McClurg, O., & Troeberg, L. (2022). The extracellular matrix of articular cartilage controls the bioavailability of pericellular matrix-bound growth factors to drive tissue homeostasis and repair. *International Journal of Molecular Sciences, 23*(11), 6003. https://doi.org/10.3390/IJMS23116003

Wang, R., Huang, X., Zoetebier, B., Dijkstra, P. J., & Karperien, M. (2022). Enzymatic co-crosslinking of star-shaped poly(ethylene glycol) tyramine and hyaluronic acid tyramine conjugates provides elastic biocompatible and biodegradable hydrogels. *Bioactive Materials, 20*, 53. https://doi.org/10.1016/J.BIOACTMAT.2022.05.020

Wu, X., He, C., Wu, Y., & Chen, X. (2016). Synergistic therapeutic effects of Schiff's base cross-linked injectable hydrogels for local co-delivery of metformin and 5-fluorouracil in a mouse colon carcinoma model. *Biomaterials, 75*, 148–162. https://doi.org/10.1016/J.BIOMATERIALS.2015.10.016

Yu, F., Cao, X., Li, Y., Zeng, L., Yuan, B., & Chen, X. (2013). An injectable hyaluronic acid/PEG hydrogel for cartilage tissue engineering formed by integrating enzymatic crosslinking and Diels–Alder "click chemistry. *Polymer Chemistry, 5*(3), 1082–1090. https://doi.org/10.1039/C3PY00869J